Chloride (HCl/Cl⁻) dominates inorganic aerosol formation from ammonia in the Indo-Gangetic Plain during winter: Modeling and comparison with observations

Pooja V. Pawar[1,6], Sachin D. Ghude[1], Gaurav Govardhan[1], Prodip Acharja[1], Rachana Kulkarni[2], Rajesh Kumar[3], Baerbel Sinha[4], Vinayak Sinha[4], Chinmay Jena[5], Preeti Gunwani[1], Tapan Kumar Adhya[6], Eiko Nemitz[7], and Mark A. Sutton[7]

[1]Indian Institute of Tropical Meteorology (IITM), Ministry of Earth Sciences, Pune, India
[2]Savitribai Phule Pune University, Pune, India
[3]National Center for Atmospheric Research (NCAR), Boulder, CO, USA
[4]Department of Earth and Environmental Sciences, Indian Institute of Science Education and Research Mohali, Punjab, India
[5]India Meteorological Department (IMD), Ministry of Earth Sciences, Lodhi Road, New Delhi, India
[6]Kalinga Institute of Industrial Technology (KIIT), Bhubaneshwar, India
[7]UK Centre for Ecology & Hydrology (UKCEH), Edinburgh, UK

Correspondence to: Sachin D. Ghude (sachinghude@tropmet.res.in)

Abstract. The Winter Fog Experiment (WiFEX) was an intensive field campaign conducted at Indira Gandhi International Airport (IGIA) Delhi, India, in the Indo-Gangetic Plain (IGP) during the winter of 2017-2018. Here, we report the first comparison in South Asia of high temporal resolution simulation of ammonia (NH_3) along with ammonium (NH_4^+) and total NH_x (= NH_3 + NH_4^+) using the Weather Research and Forecasting model coupled with chemistry (WRF-Chem) and measurements made using the Monitor for AeRosols and Gases in Ambient Air (MARGA) at the WiFEX research site. In the present study, we incorporated Model for Simulating Aerosol Interactions and Chemistry (MOSAIC) aerosol scheme into the WRF-Chem. Despite simulated total NH_x values/variability often agreed well with the observations, the model frequently simulated higher NH_3 and lower NH_4^+ concentrations than the observations. Under the winter conditions of high relative humidity (RH) in Delhi, hydrogen chloride (HCl) was found to promote the increase in the particle fraction of NH_4^+ (which accounted for 49.5 % of the resolved aerosol in equivalent units) with chloride (Cl^-) (29.7 %) as the primary anion. By contrast, the absence of chloride (HCl/Cl^-) and their chemistry in the standard WRF-Chem model results in the prediction of sulfate (SO_4^{2-}) as the dominant inorganic aerosol anion. To understand the mismatch associated with the fraction of NH_x in the particulate phase (NH_4^+/NH_x), we added HCl/Cl^- to the model and evaluated the influence of its chemistry by conducting three sensitivity experiments using the model: No HCl, Base Case HCl (using a published waste burning inventory), and 3×Base HCl run. We found that 3×Base HCl increased the simulated average NH_4^+ by 13.1 µg m⁻³ and NH_x by 9.8 µg m⁻³ concentration while reducing the average NH_3 by 3.2 µg m⁻³, which is more in accord with the measurements. Thus HCl/Cl^- chemistry in the model increases total NH_x concentration, which was further demonstrated by reducing NH_3 emissions by a factor of 3 (-3×NH_3_EMI) in the 3×Base HCl simulation. Reducing NH_3 emissions in the 3×Base HCl simulation successfully addressed the discrepancy between measured and modeled total NH_x. We conclude that modeling the fate of NH_3 in Delhi requires a correct chemistry mechanism accounting for chloride dynamics with accurate inventories of both NH_3 and HCl emissions.

1 Introduction

The Indo-Gangetic Plain (IGP) is one of the global hotspots of atmospheric ammonia (NH_3) and faces a range of environmental challenges, particularly during the winter season, including adverse air pollution episodes, especially as NH_3 plays a substantial role in secondary aerosol formation (Ghude et al., 2020, 2008b, 2008a; Kumar et al., 2021; Saraswati et al., 2019; Sharma et al., 2020; Singh et al., 2021). Atmospheric NH_3, along with oxides of nitrogen (NO_x), together account for the largest source of reactive nitrogen (N_r), which is primarily emitted by agricultural activities, livestock population, industrial activities, and transportation (Ghude et al., 2009, 2010, 2012, 2013; Móring et al., 2021; Pawar et al., 2021; Sutton et al., 2017b). Ammonia in the environment plays a crucial role in atmospheric chemistry and the eutrophication and acidification of ecosystems (Datta et al., 2012; Mandal et al., 2013; Pawar et al., 2021; Sharma et al., 2008, 2012, 2014b). Control of NH_3 becomes a key priority in an emerging international strategy to manage the global nitrogen cycle (Gu et al., 2021; Sutton et al., 2020). Ammonia is one of the important aerosol precursor gases, and ammonium (NH_4^+) is a major counter ion for the three anions such as chloride (Cl^-), nitrate (NO_3^-), and sulfate (SO_4^{2-}) contributing to $PM_{2.5}$ composition (Seinfeld et al., 2016). In addition, as the dominant alkaline gas in the atmosphere, NH_3 has attracted the interest of scientific researchers since it has been known to promote new aerosol formation both in the initial homogeneous nucleation and in the subsequent growth, especially during wintertime (Acharja et al., 2020, 2021; Ali et al., 2019; Duan et al., 2021; Wagh et al., 2021).

In this study, we focus on wintertime ~~analyses~~ since this season is characterized by low-to-dense fog events, lower temperature (T), and variability of relative humidity (RH), which fluctuates from 40 to 100 % (Ghude et al., 2017; Kumar et al., 2020). Ammonia acts as a neutralization agent for determining the acidity of aerosol particles (Acharja et al., 2020; Ali et al., 2019; Ghude et al., 2017). It also affects $PM_{2.5}$, the acidity of clouds, and the wet deposition of nitrogen by neutralizing acidic species (Gu et al., 2021; Xu et al., 2020). Increasing NH_3 concentration over Delhi compared with the surrounding area leads to an increase in $PM_{2.5}$ concentrations (Ghude et al., 2022; Sharma et al., 2008, 2012, 2014a), which in turn affects air quality, human health, and climate (Behera et al., 2013; Ghude, 2016; Ghude et al., 2008b; Nivdange et al., 2022; Sutton et al., 2017a; Sutton and Howard, 2018).

Satellite observations (Van Damme et al., 2018; Warner et al., 2017), chemical transport models (CTMs) (Clarisse et al., 2009, 2010; Wang et al., 2020b), and ground-based observations (Pawar et al., 2021) revealed that the IGP is the largest regional hotspot of NH_3 concentrations on Earth. Previous studies have identified various sources of NH_3, for example, agricultural activities, industrial sectors, motor vehicles, garbage, sewage, and urine from rural populations at the global scale (Behera et al., 2013; Huang et al., 2012; Sutton et al., 2008). However, in Delhi, agricultural activity (including surrounding arable and sub-urban livestock farming) is estimated to be the dominant source of NH_3, along with traffic emissions (Kuttippurath et al., 2020; Móring et al., 2021; Sharma et al., 2020), but its emissions are subject to large uncertainty. Globally, various modeling efforts have investigated the relative effectiveness of reducing NH_3 emissions in curtailing $PM_{2.5}$ formation (Gu et al., 2021; Pinder et al., 2007, 2008; Zhang et al., 2020). However, over India, the impact on reducing $PM_{2.5}$ might be limited because NH_3 emission reductions may be more challenging due to its ~~alkaline nature~~ diverse and area-wide sources. Ianniello et al. (2010) and Lan et al. (2021) have investigated the variation of atmospheric NH_3 at an urban and suburban site of Beijing with respect to meteorological factors, where RH was found to be a strong factor in influencing the NH_3 mixing ratio. A few studies over Asia have highlighted the gas-to-particle conversion of NH_3

79   in Delhi (Acharja et al., 2021; Saraswati et al., 2019) and China and its subsequent impact on the aerosol formation
80   (Wang et al., 2015; Xu et al., 2020). Furthermore, excess NH_3 during fog can also enhance secondary aerosol
81   formation in Delhi during winter (Acharja et al., 2021). However, the wintertime behavior of NH_3 in Delhi in
82   CTMs has not yet been investigated and remains poorly understood (Ellis et al., 2011; Metzger et al., 2006). In a
83   recent study, Pawar et al. (2021) highlighted uncertainties associated with gas-to-particle partitioning of NH_3 in a
84   global model MOZART-4 and found a significant overestimation of NH_3 in the model compared with the
85   measurements. The overestimation of NH_3 in the model led the authors to hypothesize that a source specific NH_3
86   emission inventory in India, considering agricultural statistics on fertilizer use and animal distribution, was
87   missing. Also, there was a need for a high-resolution regional model with advanced chemistry to resolve the NH_3
88   emissions on the local scale.

89   The present study utilizes the regional Weather Research and Forecasting model coupled with chemistry
90   (WRF-Chem) interpreted using measurements from the Winter fog Experiment (WiFEX), including NH_3, water-
91   soluble ions in $PM_{2.5}$, other trace gases, and meteorological parameters during December-January, 2017-18. For
92   the first time in South Asia, we discuss and compare the modeled and observed temporal variation in gaseous
93   NH_3, particulate NH_4^+, and total NH_x (= NH_3 + NH_4^+). Since we found that the total modeled NH_x matches well
94   with the observations, we investigate the ability of the model to accurately describe the gas-to-particle partitioning
95   of the measurements (MARGA) by evaluating the fraction of NH_x in the particulate phase (NH_4^+/NH_x). We
96   conducted several sensitivity experiments with and without adding anthropogenic waste burning emissions of
97   hydrochloric acid (HCl) in the model. The updated model with HCl/Cl^- chemistry was used to analyze and
98   compare the temporal variation of NH_3, NH_4^+, and total NH_x from the WiFEX measurements.

99   **2. Data and methodology**

100 **2.1 Observational datasets**

101 **2.1.1 Description of MARGA**

102   In the present study, we used the same dataset which was previously published by Acharja et al. (2020)
103 and 2021), which described the aerosol time-series and chemistry measured with a Monitor for AeRosols and
104 Gases in Ambient Air-model 2S instrument (MARGA). The MARGA system has two channels, one for sampling
105 PM_1 and the other for sampling $PM_{2.5}$ for ground-based observations. The MARGA (two sampling boxes,
106 analytical box, and connected pumps) was located inside the Indira Gandhi International Airport (IGIA), New
107 Delhi (28.56° N, 77.09° E), with the inlet PM_1 and $PM_{2.5}$ impactors fixed on the terrace with 2 m long inlet lines
108 sampling outdoor air at 8 m above ground and 2 m above the rooftop. Measurements covered a winter period (19
109 December 2017 to 21 January 2018) with frequent moderate to dense fog events. Following intake through the
110 PM_1 and $PM_{2.5}$ impactors, the air was passed through two parallel inlet tubes 2 m long and 14 mm inner diameter
111 PolyTetraFluoroEthylene (PTFE) to the PM_1 and $PM_{2.5}$ sampling channels of the MARGA. The air flow rate in
112 each MARGA sampling box is regulated to a volumetric flow of 1 m^3 h^{-1}. The measurements are close to real-
113 time, as two sets of syringes are employed to collect the samples in which a set of syringes collects the sample
114 and another set sends the collected samples from the previous hour for analysis. Each MARGA sampling system
115 consists of a steam jet aerosol collector (SJAC) and a wet rotating denuder (WRD) for collecting and measuring

116 water-soluble inorganic particulate species and gases in the ambient air. The continuous coating of the WRD by
117 a thin film of absorption solution (10 ppm hydrogen peroxide (H_2O_2)) allows the diffusion of gases into the
118 absorption solution. By contrast, the low diffusion velocity of sub-micron particles restricts the ability of water-
119 soluble aerosols to diffuse into the absorption solution. The absorption solution is continually changed to replace
120 that abstracted for ion chromatography (IC) analysis of the dissolved gases. The air stream, depleted of gases by
121 the WRD, subsequently enters the SJAC, where the steam enhances water-soluble aerosols to grow, allowing their
122 mechanical capture in a cyclone. The aqueous solutions deriving from two cyclones (for PM_1 and $PM_{2.5}$,
123 respectively) are then supplied to the IC for chemical analysis (Acharja et al., 2020).

124 Ambient surface concentrations of NH_3 along with other trace gases (HCl, nitrous acid (HONO), nitric
125 acid (HNO_3), and sulfur dioxide (SO_2) and water-soluble inorganic components of PM_1 and $PM_{2.5}$ (Cl^-, nitrate
126 (NO_3^-), SO_4^{2-}, NH_4^+, sodium (Na^+), potassium (K^+), magnesium (Mg^{2+}), and calcium (Ca^{2+}) were then quantified
127 online by anion and cation chromatography in the analytical box at an hourly resolution. We have used only $PM_{2.5}$
128 inorganic water-soluble components and the gaseous measurements (available from both the PM_1 and $PM_{2.5}$
129 MARGA collection systems). Since NH_4^+ with the three major anions: Cl^-, NO_3^- and SO_4^{2-} constituted 97.3 %
130 of the total measured ions in $PM_{2.5}$ (Acharja et al., 2020), we consider these four significant ions in our present
131 study. In contrast, the remaining ionic species (i.e., Na^+, K^+, Mg^{2+}, and Ca^{2+}) contributed only about 3 % of the
132 total measured ions and were neglected as it would not impact our present study significantly (Acharja et al.,
133 2020). Anions are separated in a Metrosep A Supp-10 (75/4.0) column with sodium carbonate (Na_2CO_3) and
134 sodium bi-carbonate ($NaHCO_3$) (7/8 mmol l^{-1}) eluent. Whereas for cations separation, a Metrosep C4 (100/4.0)
135 cation column with 3.2 mmol l^{-1} HNO_3 eluent was used (Acharja et al., 2020). To suppress the eluent background
136 conditivity of anion chromatographs, three ion exchange units were used to ensure that the ion exchange unit is
137 regenerated in each analysis. 1 M Phosphoric acid (H_3PO_4) was used for this purpose. This was performed to
138 improve the signal-to-noise (S/N) of the anion chromatographs. Details of the MARGA instrument can be found
139 in Makkonen et al. (2012), Thomas et al. (2009), Twigg et al. (2015).

2.1.2 Quality assurance/quality control (QA/QC) of MARGA

141 To ensure the observation's accuracy and check the data's quality, we have ~~taken~~ followed best practices ~~all the~~
142 ~~precautionary measures~~ during the study. The eluents, absorption, and regenerant solutions were prepared with
143 minimum manual intervention. The operational parameters like anion ~~and,~~ cation conductivity, SJAC heater
144 temperature, column oven temperature, and airflow were regularly monitored to keep them within the safe limit.
145 In addition to these, before injection of each sample into the anion and cation IC columns, the Lithium Bromide
146 (LiBr) internal standard solution containing 320 µg l^{-1} lithium (Li^+) and 3680 µg l^{-1} bromide (Br^-) was mixed with
147 each sample to provide calibration of each analysis. This ensures that each analysis is calibrated, and the
148 concentration of gaseous and ionic samples are measured accurately. The PM_1 and $PM_{2.5}$ impactors were typically
149 cleaned fortnightly to remove any material that may have ~~stuick~~ on the surface and inlets of the impactors. The
150 lower detection limits (LODs) of the species monitored by MARGA were mentioned in Acharja et al. (2021). It
151 shows that concentrations of species like Cl^-, NO_3^-, SO_4^{2-}, NH_4^+, SO_2, and NH_3 were always higher than LODs
152 during the winter period. But, concentrations of species like Na^+, K^+, Ca^{2+}, Mg^{2+}, HCl, HONO, and HNO_3 were
153 sometimes below LODs, but the fraction of it was less than ~10 % of the total observation period. We have omitted
154 these values and treated them as NA. As the fraction of observational hours is less and these species contribute

155 much less to the PM_1 and $PM_{2.5}$ mass concentrations, we believe below LODs values would not significantly
156 deviate our results. The quality of the data obtained was then checked using the ion-balance method. As an
157 additional quality check, the ratio of the sum of cations to anions (neq m^{-3}) was used as an indicator for the viable
158 data. We have checked the cation-to-anion ratio of each hourly sample expressed in the unit of neq m^{-3}. We
159 accepted only those values near to unity and rejected those not within the 10 % error bar limit. Based on this
160 evaluation method, overall, for the campaign, the ratio was near unity (1.06 for PM_1 and 0.96 for $PM_{2.5}$). Excellent
161 charge balance between anions and cations measured by the system also confirms that there are no significant
162 contamination issues associated with the aerosol measurements. Values in slight excess of unity may indicate the
163 presence of formate and acetate in the aerosol, which MARGA does not measure. Further detail on the quality
164 control of MARGA can be found in Acharja et al. (2020).

2.1.3 Other ground-based measurements

166 Hourly NO_x measurements were made by the chemiluminescence method, and hourly ozone (O_3) measurements
167 were made by the UV photometric method (CPCB, 2011) at the nearest air quality monitoring station (AQMS) of
168 IGIA operated by the Central Pollution Control Board (CPCB). CPCB follows the United States Environmental
169 Protection Agency (USEPA) approved AC32M NO_x and 42M O_3 analyzer manufactured by Environment S. A.
170 India Private Limited. We used one-hour monitored NO_x and O_3 values in our study. These air quality monitoring
171 stations' quality control and assurance processes were followed as outlined in CPCB (2014, 2020). For data quality
172 of CPCB, we omitted all those observed values which fell below LOD of the instrument (2 µg m^{-3} for NO_x and 4
173 µg m^{-3} for O_3) (Technical specifications for CAAQM station, 2019) and above 500 µg m^{-3} for NO_x and 140 µg m^{-3}
174 ^{3} for O_3 and treated them as NA at a given site. For the NO_x and O_3 datasets, only a small fraction of data (2 %)
175 were outside the instrument operating ranges specified. This step aims to remove any short-term local influence
176 that the models cannot capture and retain the regional-scale variability because the nearest sites are located in the
177 urban environment. We removed a single spike represented by a change of more than 100 µg m^{-3} in just 1 hour
178 (h) for all the data in CPCB monitoring stations to filter out random fluctuations in the observations. We removed
179 some very high NO_x and O_3 values that appeared in the time series right after measurement gaps. Meteorological
180 parameters, including air temperature (T), relative humidity (RH), wind speed, and wind direction, were measured
181 with the automatic weather station (AWS) platform on a 20 m flux tower (Ghude et al., 2017). For detailed
182 information on the measurement site and its meteorological parameters, refer to (Ali et al., 2019).

2.2 WRF-Chem v 3.9.1 model

184 The Weather Research and Forecasting model coupled with chemistry (WRF-Chem v3.9.1) was employed in this
185 study to simulate atmospheric gases and aerosols over Delhi during the peak winter period, starting from 19
186 December 2017 to 21 January 2018. We recently used a similar model configuration to simulate the air quality
187 over Delhi (Ghude et al., 2020; Kulkarni et al., 2020). This study used the Model for Ozone And Related chemical
188 Tracers (MOZART-4) gas-phase chemical mechanism coupled with the Model for Simulating Aerosol
189 Interactions and Chemistry (MOSAIC) aerosol scheme, that simulates SO_4^{2-}, NH_4^+, NO_3^-, methanesulfonate, Na^+,
190 Ca^{2+}, Cl^-, carbonate, black carbon (BC), and primary organic mass (OC). Other inert minerals, trace elements, and
191 inorganic species are lumped together as different inorganic masses. MOSAIC allows gas-to-particle formation,
192 which includes NH_3, HCl, sulfuric acid (H_2SO_4), HNO_3, and methane sulfonic acid (MSA), and also includes

193 secondary organic aerosols (SOA). Aerosol size distributions are represented by a sectional aerosol bin approach
194 with four size bins (Georgiou et al., 2018). MOSAIC incorporates the thermodynamic and gas-particle partitioning
195 module described by Zaveri et al. (2008). To reduce the computational cost, we selected a 4-bin MOSAIC
196 mechanism that simulates thermodynamic equilibrium and other aerosol processes such as condensation,
197 coagulation, and nucleation. The same mechanism has been widely used with WRF-Chem for simulations outside
198 India (Bucaram and Bowman, 2021; Sha et al., 2019; Yang et al., 2018), but only a limited number of studies
199 have applied it to the Indian domain to include more detailed chemistry and species (Gupta and Mohan, 2015;
200 Jena et al., 2020; Kumar et al., 2018). The SOA formation in MOSAIC is simulated using the volatility basis set
201 approach (Knote et al., 2015). For consistency with the $PM_{2.5}$ MARGA measurements, we have chosen 3-bins
202 according to simulated aerosols size (0.04–0.156 μm; 0.156–0.625 μm; 0.625–2.5 μm) in accordance with the
203 WRF-Chem aerosol size distribution.

204   The model domain covers the entire northern region of India, but here model simulations are compared
205 with the observations at IGIA, New Delhi (28.56° N, 77.09° E). The domain was set with a horizontal grid-spacing
206 of 10 km in both the latitudinal and longitudinal directions. The model top vertical grid included 47 vertical levels,
207 with the model top set to 10 hPa. The physical parameterization schemes of model configuration are the same as
208 those described by Ghude et al. (2020) and Jena et al. (2021). EDGAR-HTAP (Emission Database for Global
209 Atmospheric Research for Hemispheric Transport of Air Pollution) for the year 2010 at 0.1° x 0.1° grid resolution
210 was used in this study for anthropogenic emissions of aerosols and trace gases ($PM_{2.5}$, PM_{10}, OC, BC, CO, NO_x,
211 etc.) and are scaled to 2018 as per Jena et al. (2021). Biogenic emissions are calculated online using the Model of
212 Emissions of Gases and Aerosols from Nature version 2.1 (MEGAN2.1) (Guenther et al., 2006), and dust
213 emissions are based on the traditional Goddard Global Ozone Chemistry Aerosol Radiation and Transport
214 (GOCART) dust scheme that works with MOSAIC (Ginoux et al., 2001). Fire INventory from NCAR (FINNv1.5)
215 was used in this study for daily open biomass burning emissions that are vertically distributed within the model
216 using Freitas et al. (2007). The chemical initial and lateral boundary conditions come from the global model
217 simulations from the Model for Ozone and Related Chemical Tracers (MOZART-4), and the meteorological initial
218 and lateral boundary conditions are provided from the fifth generation European Centre for Medium-Range
219 Weather Forecasts (ECMWF) atmospheric reanalysis of the global climate (ERA5) with six-hourly temporal
220 resolution. The simulations were reinitialized every fifth day to limit the growth of meteorological errors in our
221 simulations, but the chemical fields were carried forward from the previous simulation.

222 **3. Results and Discussion**

223 **3.1 Comparison of temporal variation in NH_3, NH_4^+, and total NH_x using WRF-Chem and MARGA**

224 **3.1.1 Diurnal variation**

225 To investigate how well a state-of-the-art chemical transport model performs in capturing the diurnal behavior of
226 NH_3 and NH_4^+, we compared observed and model-simulated diurnal profiles of NH_3 and NH_4^+. Figure 1 displays
227 the comparison of diurnal variation (00:00 to 23:00 Indian Standard Time (IST)) in meteorological parameters (T
228 and RH) at the IGIA site in Delhi (Fig. 1a) along with NH_3 and NH_4^+ averaged over the study period (Fig. 1b)
229 between observations and model. We adopted diurnal variation in emissions from a recent study by Jena et al.

230   (2021). Note that diurnal variability in the model simulations is primarily controlled by the planetary boundary

231   layer mixing. We first investigated the ability of WRF-Chem to accurately predict the meteorological parameters

232   of RH and T, which are important determinants of the gas-to-aerosol partitioning of (semi-) volatile compounds.

233   As shown in Fig. 1a, simulated T and RH are in reasonable agreement with the observations, with the simulated

234   RH values falling in the range of 50–90 %. Overall, it can be seen that the model shows cold and wet bias compared

235   to the observations but shows warm bias (about 2-3 °C) and dry bias (about 10-12 %) in the afternoon hours. In

236   spite of the small change in the amplitude of the diurnal cycle of RH, the phase characteristics of the diurnal cycle

237   of both T and RH are reasonably well captured by the model. Figure 1b shows that simulated NH_3 and NH_4^+ are

238   very different compared with the MARGA measurements. The model predicts an average NH_3 and $NH_4^+ \pm 1\sigma$

239   mass loading of 56.7 ± 14.3 and 14.7 ± 4.9 µg m^{-3}, respectively, while MARGA measurements indicate an average

240   NH_3 and $NH_4^+ \pm 1\sigma$ mass loading of 28.2 ± 12.4 and 36.9 ± 15.1 µg m^{-3}, respectively. We find the diurnal variation

241   of gas-phase NH_3 is significantly overestimated by the model (Normalised Mean Bias (NMB) = 1.02). On the

242   contrary, NH_4^+ is underestimated by about 60 % (NMB = -0.60). Simulated NH_3 concentrations peak between

243   07:00-09:00 and 22:00-23:00 h with bimodal variation, whilst MARGA shows a single peak around 12:00-13:00

244   h. On the contrary, a nearly flat diurnal profile of NH_4^+ is predicted by the model, whereas the average MARGA

245   NH_4^+ concentration maxima and minima were observed during night-time (16:00-03:00 h) and daytime (03:00-

246   08:00 and 09:00-16:00 h), respectively.

247   We also looked into the average diurnal profile of NO_x and ~~the~~ NH_3 during dense fog events, and the

248   details can be found in the supplement (Fig. S1 and S2 in the Supplement). It is evident that the observed daytime

249   peak of NH_3 did not coincide with NO_x peaks, suggesting that traffic emissions do not contribute significantly to

250   the observed NH_3 rise. The observed correlation between fog water and enhanced NH_3 pulses is consistent with

251   what would also be expected from the evaporation of dew (Sutton et al., 1998; Wentworth et al., 2014, 2016) (S2

252   in the Supplement) but is not sufficient to identify whether it is the main cause of the daytime increase of NH_3. In

253   the future, measurements of the dew water NH_4^+ and the accumulation of dew water would be ideal for

254   illuminating the contributing processes. The daytime increase in NH_3 concentration could be associated with NH_4^+

255   aerosol volatilization driven by an associated sharp change in T and RH (~ 11:00-12:00 h) (Sutton et al., 2009a,

256   2013) off-ground surfaces. The fastest increase in T is 12:00 h, which is indeed when NH_3 was at maximum

257   concentration indicating gas-to-particle partitioning may impact the diurnal behavior of NH_3 at Delhi during

258   winter (Sutton et al., 2009a, 2009b). However, in the model, because the largest increase in simulated NH_3 also

259   precedes the large changes in simulated meteorological parameters, and because the simulated particulate NH_4^+

260   is flat compared to observations, simulated meteorology is ruled out as a significant contribution to high bias in

261   simulated NH_3. Also, the current model does not include the bidirectional exchange of NH_3 with surfaces such as

262   dew and fog water.

263   **3.1.2 Daily mean variation**

264   To assess the validity of the model, the ratio between simulated and observed ~~the ratio between observed~~

265   ~~and simulated values~~ (model/obs) was tested. Figure 2 displays the model/obs ratio of daily mean variations in

266   the NH_3, NH_4^+, and total NH_x concentrations. The model shows large differences in NH_3 and NH_4^+ compared with

267   observations. We find a model/obs higher than 1 (1.5-4.5) in simulated NH_3, indicating the model is biased high

268   (NMB = 1.02), while there is a poor agreement for NH_4^+ (model/obs less than 0.5), indicating model is biased low

269 (NMB = -0.62). There is good agreement between the modeled total NH_x, which is mostly consistent with the

270 observation (model/obs close to 1) with a small bias (NMB = 0.08). Despite the adequate ability of the model to

271 reproduce the accurate total NH_x, the model is biased low for NH_4^+ and high for NH_3, indicating that the model's

272 representation of the gas-to-particle partitioning is not correct. It is, therefore, necessary to understand missing

273 chemical processes in gas-to-particle partitioning responsible for the overestimation of NH_3 and underestimation

274 of NH_4^+ in the model.

3.2 Gas-to-particle partitioning

276 We investigated the ability of the model to accurately describe the gas-to-particle partitioning of the measurements

277 (MARGA) by evaluating the fraction of total NH_x in the particulate phase (NH_4^+/NH_x) (Ellis et al., 2011; Wang

278 et al., 2015) for which statistical values are summarized in Table 1. The correlation coefficient (r) indicates an

279 inverse relationship of NH_4^+/NH_x with NH_3 for both MARGA and model (r = -0.57, -0.58, respectively). A strong

280 correlation of the MARGA ratio NH_4^+/NH_x with the dominant anion concentration (Cl^-: r = 0.79) was observed.

281 However, the measurement shows a poor relationship between SO_4^{2-} and NH_4^+/NH_x followed by NO_3^-, which is

282 probably due to very low concentrations that do not change NH_4^+/NH_x significantly even when SO_4^{2-} and NO_3^-

283 are neutralized (see Fig. 6). By contrast, the model shows a strong correlation between NH_4^+/NH_x with SO_4^{2-}

284 concentration (r = 0.77). MARGA indicates high particulate fractions of NH_4^+ and Cl^- while the modeled

285 composition is dominated by NH_4^+ and SO_4^{2-}. This mismatch is due to the complete absence of Cl^- chemistry in

286 the standard model. The measured NH_4^+/NH_x suggests that anthropogenic HCl may be promoting this increase in

287 particle fraction of NH_4^+ and Cl^- via partitioning into the aerosol, deprotonating in the aerosol water, followed by

288 NH_3 partitioning and being protonated by the ionization of the strong electrolyte HCl (Chen et al., 2022; Gunthe

289 et al., 2021).

290 Figure 3 shows the percentage contribution of gases (NH_3, SO_2, HCl, HNO_3, and HONO) and $PM_{2.5}$

291 aerosol (NH_4^+, SO_4^{2-}, NO_3^- and Cl^-) during the WiFEX measurements. The pie charts for the gases show that NH_3

292 (accounting for 53.3 % of the measured total gas concentration) dominates the gas phase, followed by sulfur

293 dioxide (SO_2) (35.61 %), whereas $PM_{2.5}$ aerosol show NH_4^+ (49.5 %) as a major cation and Cl^- (29.7 %) as a

294 significant anion followed by NO_3^- (11.7 %) and SO_4^{2-} (9 %). There is also a very high amount of SO_2 reaching

295 the site from the nearby industrial area, which is not converted to SO_4^{2-} very quickly (Acharja et al., 2021). In a

296 normally NH_3-rich atmosphere, gas-phase oxidation of SO_2 is much slower than the aqueous phase oxidation by

297 ~~of~~ O_3, and due to nearby sources, much of the sulfur is present as SO_2 (Li et al., 2007). ~~(Fig. S3 in the Supplement).~~

298 This appears to be because of the slow rate of gas phase oxidation of SO_2. Although the atmosphere is rich in

299 NH_3, in principle favoring aqueous phase oxidation via O_3, it appears that O_3 concentrations are often insufficient

300 (mean = 36.3, median = 33.8, minimum = 26.5, and maximum = 53.9, ug m^{-3} respectively) at the IGIA site (Fig.

301 S3 in the Supplement). Hence for many periods during the WIFEX campaign, SO_4^2 and NO_3^- are very low, with

302 the result that the NH_4^+/NH_x ratio does not change appreciably when SO_4^{2-} is neutralized (Table 1).

303 According to thermodynamic equilibrium theory, an aqueous solution maintains charge neutralization

304 initially by balancing NH_3 uptake with the uptake of sulfuric acid (H_2SO_4) before HNO_3 and HCl can partition

305 into the aqueous aerosol; hence all SO_4^{2-} in the condensed phase will be fully neutralized before any HNO_3, or

306 HCl can partition (Behera et al., 2013). Typical Delhi winter conditions of excess NH_3, high RH, and low T favor

307 gas-to-particle partitioning of NH_3. The principal inorganic chemical reactions that occur in aqueous atmospheric

308 aerosols form pairs of non-volatile NH_4^+ and acid anions (SO_4^{2-}, NO_3^-, and Cl^-) are summarized in reactions R1

309 to R3 (Seinfeld et al., 1998).

310 $2NH_{3(g)} + H_2SO_{4(g)} \rightleftarrows NH_4^+ + SO_4^{2-}$ (R1)

311 $NH_{3(g)} + HNO_{3(g)} \rightleftarrows NH_4^+ + NO_3^-$ (R2)

312 $NH_{3(g)} + HCl_{(g)} \rightleftarrows NH_4^+ + Cl^-$ (R3)

313

314 NH_4^+ and Cl^- (R3), which are favored by low T and high RH, form a reversible equilibrium with NH_3 and HCl

315 (Ianniello et al., 2011; Seinfeld and Pandis, 2016), which was the case during WiFEX. It is likely that high Cl^- in

316 Delhi resulted from gas–to-particle partitioning of HCl into aerosol water in the presence of excess NH_3 (R3),

317 with aqueous phase Cl^- stimulating further water uptake and jointly driving aerosol mass composition and growth

318 through co-condensation (Chen et al., 2022; Gunthe et al., 2021). Hence, to understand the driver of the measured

319 NH_4^+ and the role of aqueous chemistry, we plotted the fraction of the ratio of HCl to Cl^- (HCl/Cl^-) as a function

320 of NH_4^+ concentration and RH in Fig. 4. The decrease in the fraction of HCl/Cl^- is associated with an increase in

321 NH_4^+ concentration at high RH between 70-100 %. Fraction of particulate phase Cl^- increases at high RH between

322 70-100 % and thus increases the NH_4^+ concentration. The HCl/Cl^- is highly anticorrelated (r = -0.53) with NH_4^+

323 concentration in the presence of high RH (70-100 %), further supporting the view that HCl promotes the increase

324 in the particle fraction of NH_4^+ (49.5 %) with Cl^- (29.7 %) the primary anion.

325   We investigated the directions of local emission sources associated with concentration increases of NH_3,

326 NH_4^+, Cl^- and NH_x through bivariate polar graphs using the OpenAir software (Carslaw and Ropkins, 2012) at the

327 IGIA site. Figure 5 shows the bivariate polar plots of mean NH_3 (Fig. 5a), NH_4^+ (Fig. 5b), Cl^- (Fig. 5c), and total

328 NH_x (Fig. 5d) concentration for the observation period in relation to wind speed and wind direction. The 270-300°

329 sector dominated the wind direction at IGIA (Acharja et al., 2021). Figure 5a shows that the highest NH_3

330 concentration was associated with the winds coming from the east and southeast of the site, where it could have

331 been emitted from dairy farms, including animal houses, yards, and manure storage, as well as by the application

332 to the farmland of urea and other ammoniacal fertilizers, ammoniacal wastes and ruminant urine located at this

333 region (Hindustan Times, 2021; Leytem et al., 2018; Sherlock et al., 1994). Such sources of NH_3 volatilization

334 (Hristov et al., 2011; Laubach et al., 2013) can also explain the higher concentrations of total NH_4^+ (and, by

335 definition NH_x) for air coming from the southeast of the measurement site (Fig. 5b and d). This enhancement in

336 the southeast region is not only affected by emissions but also by meteorology and chemistry. Thus higher NH_3

337 concentration may also be due to the lack of turbulent mixing, which restricts the dilution of plumes from local

338 point sources at lower wind speeds (Ianniello et al., 2010). The bivariate polar plots of NH_4^+ (Fig. 5b) and Cl^-

339 (Fig. 5c) concentration point to the west direction as a principal source for thermodynamic partitioning of NH_3

340 and HCl to the condensed phase to form NH_4^+ and Cl^-. Two industrial sources are located in this direction: the

341 site is impacted by a cluster in northwest Delhi of industrial processes, such as steel pickling industries, and others

342 include metal finishing and electroplating, which are known to be vital HCl emitters (Acharja et al., 2021;

343 Jaiprakash et al., 2017). Near the source, abundant quantities of NH_3 may drive the partitioning of HCl to the

344 condensed phase resulting in high concentrations of NH_4^+ and Cl^- towards the west at lower wind speeds. Thus,

345 high NH_4^+ and Cl^- correspond to the lowest NH_3 concentration region (inverse relation), which can be observed

346 in Fig. 5a, b, and c, highlighting the importance of nearby HCl industrial sources in driving the particle fraction

347 of NH_4^+ and Cl^-.

348   To gain insight into the role of NH_4^+ in the neutralization of anions (SO_4^{2-}, NO_3^- and Cl^-), the aerosol

349   neutralization ratio (ANR) was calculated using the observed data. The ANR is defined as the equivalent ratio of

350   NH_4^+ to the sum of SO_4^{2-}, NO_3^- and Cl^- because these species represent the dominant cations and anions in $PM_{2.5}$,

351   respectively. Figure 6 demonstrates, on average, how well the charge balance works between Cl^-, NO_3^- and SO_4^{2-}

352   (in μeq m^{-3}) as the anions and NH_4^+ as the major cation (ANR close to unity), with Cl^- as the most significant

353   anion followed by NO_3^- and SO_4^{2-}. The mean $\pm$ 1σ ANR value for $PM_{2.5}$ during the observed period was $0.96 \pm$

354   0.14. It ranges from a minimum of 0.35 ± 0.04 to a maximum of 2.31 ± 0.08. Higher values than unity may indicate

355   the presence of organic acids in the aerosol, which MARGA does not measure (Acharja et al., 2020). Also, high

356   standard error in Fig.6 indicates the possibility of uncertainties associated with the breakthrough of NH_3 spikes on

357   the denuder at high concentration ($\sim$ 1 %) (Stieger et al., 2019). However, the good charge balance indicates this

358   wasn't a major issue. There also were certain periods where low concentrations were observed of Cl^- and NO_3^-

359   (03-06 January 2018 and 16-17 January 2018) in Fig. 6. Comparing the model/obs for NH_3, NH_4^+ and total NH_x

360   during these periods provides some degree of validation of the model where sulfur chemistry dominates the

361   reaction with NH_3. Figure S4 (in the supplement) shows that model/obs indicates substantial variability which

362   appears to be overestimating NH_3 (model/obs >1) while underestimating total NH_4^+ (model/obs <1) on average

363   in the model.

3.3 Influence of HCl/Cl^- chemistry in WRF-Chem

365   We further conducted three scenario simulations for the period 7-16 January 2018 (10 days) to explore the

366   potential impacts of the addition of anthropogenic chloride (HCl/Cl^-) emissions in the concentrations of NH_3,

367   NH_4^+ and total NH_x. We employ the HCl emissions from trash-burning activities in Delhi, as predicted by Sharma

368   et al. (2019) in our model set-up. We tested the three sensitivity experiments named: No HCl (0 mol km^{-2} h^{-1}),

369   Base Case HCl ($3\times$ Sharma et al., 2019; 24.8 mol km^{-2} h^{-1}), and $3\times$Base HCl (74 mol km^{-2} h^{-1}) scenario, reflecting

370   adjustments which are consistent with the more recent upward adjustments in the amount of waste burned in

371   landfills by Chaudhary et al. (2021) and also to reflect additional industrial HCl sources not accounted for in the

372   inventory. Figure 7 presents the box-whiskers plots for secondary inorganic aerosols and trace gases from the

373   observations (MARGA), and those simulated by the model for the three sensitivity experiments. Daily mean $\pm$ 1σ

374   values are summarized in Table 2 for three different model scenarios. As can be observed from Fig. 7(a-c),

375   increasing the HCl emissions (Fig. 7g) in the model partitions more NH_3 to the condensed phase due to its high

376   concentrations, reaching maximum mass loadings of NH_4^+ and Cl^- of 70 and 110 μg m^{-3}, respectively, in the

377    $3\times$Base HCl scenario, while increasing the total mean NH_x concentration by 15 μg m^{-3} compared to the No HCl

378   run presumably reflecting the longer residence time of NH_4^+ for near-surface air measurements.

379   The simulated NO_3^- concentration (Fig. 7e) generally exceeds the measurements in all three experiments;

380   since the main neutralizing species for NO_3^- is NH_4^+, it is controlled via the equilibrium between NO_3^-, HNO_3, and

381   NH_3, but also the competition with HCl for free NH_3. Simulated HNO_3 is significantly underestimated (by $\sim$3 μg

382   m^{-3}) (Fig. 7h) by the model compared to the observations. As a consequence, the model suggests that NO_3^-

383   formation from gaseous NH_3 and HNO_3 cannot occur. The gas fraction of observed HNO_3 will be determined by

384   aerosol pH and liquid water content based on NH_3 and NO_3^- availability (Nenes et al., 2020). The over-prediction

385   of NH_3 concentration in the model compared with the observations generates more NO_3^- (and simultaneously

386   reduces HNO_3), with the total fraction of HNO_3 + NO_3^- (THNO3) concentration in the model also exceeding the

387 observed THNO$_3$, which is more strongly affected by reducing the NH$_3$ emissions in the model (Fig. S5 in the

388 Supplement). On average, THNO$_3$ reduced by only 0.38 µg m^{-3} in 3×Base HCl compared to the No HCl run. But

389 reducing NH$_3$ emissions by a factor of 3 (-3×NH$_3$_EMI) in the 3×Base HCl scenario reduced mean THNO$_3$ by a

390 further 4.71 µg m^{-3}. The extent of partitioning and accumulation of NH$_4$NO$_3$ depends on T, aerosol water, pH, as

391 well as NH$_3$ availability (Nenes et al., 2020). Our model simulations find that the presence of HCl/Cl$^-$ does not

392 significantly alter THNO$_3$ but that the excess NH$_3$ with missing chloride chemistry is a major contributor and will

393 lead to mismatches in the model between measured simulated gas and particulate matter concentrations.

394   The simulated SO$_4^{2-}$ concentration (Fig. 7f) was underestimated (by ~ 7.5 µg m^{-3}), while gas-phase SO$_2$

395 Fig. 7i) was found to be overestimated by about 16 µg m^{-3} in all three experiments compared with the observations.

396 This may be caused by the fact that the drivers for typical sulfate production via OH or aqueous H$_2$O$_2$ oxidation

397 pathway are likely to be wrong in the model. The missing chemistry may underly this mismatch and requires

398 further sensitivity studies considering different SO$_2$ oxidation pathways. This requires further study, such as

399 scenario evaluation of altered SO$_2$ emissions in the model, to examine the main pathway(s) for SO$_2$ to SO$_4^{2-}$

400 conversion. Measurements of OH and other radicals in Delhi are currently lacking, making it difficult to constrain

401 the associated chemical schemes. To investigate the further impact of 3×Base HCl in the model, uptake of gaseous

402 NH$_3$ to form NH$_4^+$ and Cl$^-$ was analyzed via a strong correlation coefficient values of r = 0.84 for NH$_4^+$/NH$_x$ with

403 Cl$^-$ concentration, indicating a fraction of gas-to-particle conversion in the model correlates well with the Cl$^-$

404 concentration and was reasonably well simulated in the 3×Base HCl run.

405 **3.4 Comparison of the temporal variation in NH$_3$, NH$_4^+$, and NH$_x$ using WRF-Chem (HCl/Cl$^-$) and**
406 **MARGA**

407 **3.4.1 Diurnal variation**

408 Here, diurnal variations of monitored aerosol compounds and gases were analysed to investigate the gas-to-

409 particle conversion of NH$_3$ in the model. We analyzed the simulation results of the 3×Base HCl run**.** The diurnal

410 variations for NH$_3$ and NH$_4^+$ are controlled mainly by thermodynamic gas-to-particle partitioning, boundary layer

411 mixing, emission and deposition processes, along with vertical and horizontal advection (Meng et al., 2018).

412 Figure 8 (top) presents the diurnal variations of NH$_3$ and NH$_4^+$ (in µg m^{-3}) along with particulate NH$_4^+$, Cl$^-$, NO$_3^-$

413 , SO$_4^2$, SO$_2$, HCl, and HNO$_3$ concentrations (in µeq m^{-3}) measured (Fig. 8a (top)) and modeled (Fig. 8b (top))

414 along with its meteorological parameters such as T and RH (Fig. 8 (bottom)). We adopted diurnal variation in

415 emissions from Jena et al. (2021) based on boundary layer mixing. It can be seen in Fig. 8a (top and bottom) that

416 a much bigger peak in NH$_3$ concentration is observed in the daytime than the modeled (despite turbulence

417 differences), indeed suggesting a much stronger NH$_3$ in the middle of the day (11:00-01:00 h). As evaporation

418 proceeds mainly in the morning (08:00-12:00) getting warmer, the peak is near midday (11:00-13:00 h), rather

419 than in the afternoon (13:00-14:00 h) when warmest, similar to what was also observed in Sutton et al. (1998).

420 Indeed, the decreasing NH$_4^+$ and Cl$^-$ during the late morning (10:00 h) corresponds to the increasing NH$_3$ peak,

421 which reflects the fact that warming promotes the shift of aerosols to the gas phase. Ammonium decreases more

422 than NH$_3$ during the day, as this also evaporates to form NH$_3$. Similarly, Cl$^-$ evaporates during the day since the

423 HCl concentration increases. However, it can be seen that NO$_3^-$ and SO$_4^{2-}$ are slightly changed diurnally, inferring

424 longer range transport perhaps, whereas HCl and Cl$^-$ are from more local sources. The diurnal variability in gases

425 and aerosols in 3×Base HCl simulations in Fig. 8b (top) is primarily controlled by the planetary boundary layer

426   mixing, meteorology/dispersion, environment (T and RH in Fig. 8b (bottom)), and transport. So presumably,

427   maximum NH_3 at 08:00 h is due to limited turbulence/boundary layer, with dilution by mixing after 08:00 h.

428   However, the model is able to represent well the diurnal variation of NH_4^+ and Cl^- both in terms of amount and

429   pattern, which was not the case in the No HCl run where NH_4^+ was observed to be flat in Section 1. During the

430   hours of 09:00 and 11:00 h, when measured NH_3 rises, the model predicts a large decrease in NH_3, while during

431   19:00-23:00 h, when measured NH_3 decreases, the model predicts a large increase. Furthermore, the modeled HCl

432   and HNO_3 are very low compared to the measurements, whereas SO_2 concentration matches well with the

433   observations. It can be seen that NO_3^- and SO_4^{2-} are flat in the model. This highlights the need to develop accurate

434   diurnal variability in NH_3 emissions over this region.

435   Figure 9 presents the differences in diurnal variation of mean NH_3 (Fig. 9a), NH_4^+ (Fig. 9b), and total

436   NH_x (Fig. 9c) concentration for the three sensitivity experiments. While the simulated NH_3 concentrations

437   decrease in the 3×Base HCl compared to the No HCl and Base Case HCl run (Table 2), none of the model

438   experiments capture the diurnal cycle of NH_3. Higher levels of observed NH_3 during daytime and modeled NH_3

439   during night-time highlight the need to improve diurnal variability in NH_3 emissions over this region based on the

440   nature and strength of the actual sources. Between the No HCl and the 3xBase HCl run, the NMB for NH_3 reduced

441   from 1.38 to 1.13, and NMB for NH_4^+ systematically improved from -0.61 to -0.03. In contrast, NMB for total

442   NH_x increased from 0.12 to 0.39. Table 3 summarizes the statistical indicators for the three sensitivity

443   experiments. An increase in HCl emissions in the 3×Base HCl leads to a higher mass concentration of NH_4^+ and

444   Cl^-, which also increases total mean NH_x concentration by 22.4 µg m^{-3}, presumably reflecting the longer

445   atmospheric lifetime of NH_4^+ compared with NH_3. We find consistent high bias in all the simulations for NH_3,

446   which is highest during the early morning and at night-time. In order to better understand the relationship between

447   NH_3, NH_4^+ and NH_x concentrations in the diurnal profile of model, one sensitivity study is conducted in the best

448   case HCl experiment to simulate the response of NH_x concentrations by changing NH_3 emissions. In these

449   simulations, only NH_3 emissions were reduced further by a factor of 3 (-3×NH_3_EMI) in the 3×Base HCl

450   experiment, while all other processes and chemical schemes were unchanged. Figure S6 in the Supplement shows

451   the diel profile of model/obs ratio for NH_3 (Fig. S6a), NH_4^+ (Fig. S6b), and total NH_x (Fig. S6c) concentration

452   simulated with the 3×Base HCl and -3×NH_3_EMI scenario. Reducing NH_3 emissions in the model (-3×NH_3_EMI)

453   significantly improves model-measurement agreement for NH_3 (mean model/obs = 1.9), NH_4^+ (mean model/obs

454   = 0.9), and total NH_x concentration (mean model/obs = 1.2) compared to the 3×Base HCl run, further suggesting

455   that the longer lifetime of NH_4^+ may be the controlling driver for the total NH_x concentration in the model.

456   **3.4.2 Variation of daily means**

457   Figure S7 in the Supplement illustrates a time-series graph that compares daily mean NH_3 (Fig. S7a), NH_4^+

458   (Fig. S7b), and total NH_x concentrations (Fig. S7c) for the three sensitivity experiments, and Table 2 shows the

459   mean ± 1σ of these variables. The results show that compared to the No HCl run, NH_3 mean concentrations

460   decreased by 2 µg m^{-3} in the Base Case HCl and decreased by a further 3.2 µg m^{-3} in the 3×Base HCl run. On the

461   contrary, NH_4^+ mean concentration increases in the Base Case HCl by 7.5 µg m^{-3} and further increases by 13.1

462   µg m^{-3} (3×Base HCl). This decrease in NH_3 is associated with the enhanced gas-to-particle conversion of NH_3 to

463   NH_4^+. Associated with these changes, total mean NH_x also increased by 5.5 and 9.8 µg m^{-3} in the Base Case HCl

464   and 3×Base HCl, respectively, compared to the No HCl. This is likely due to associated increases in the

Formatted: Font color: Red

Formatted: Font color: Red

Formatted: Font color: Red

Formatted: Font color: Red

Formatted: Font color: Red

Formatted: Font color: Red

Formatted: Font color: Red

465 atmospheric lifetime of NH_x with respect to deposition as the partitioning shifted from the faster depositing gas

466 phase to the aerosol phase. The lifetime of NH_3 is very short, a few hours, while that of NH_4^+ is 1 to 15 days

467 (Aneja et al., 1998; Nair and Yu, 2020; Pawar et al., 2021; Wang et al., 2020a).

468 To understand further the overestimation of total NH_x in the daily mean variation by the model, we

469 compared 3×Base_HCl and −3×NH₃_EMI sensitivity experiment. performed a sensitivity test with the HCl

470 emissions that led to the best model/obs comparison (3×Base HCl emissions) by additionally reducing NH_3

471 emissions by a factor of 3 (-3×NH₃_EMI). Figure 10 shows the ratio of model/obs for NH_3 (Fig. 10a), NH_4^+ (Fig.

472 10b) and total NH_x (Fig. 10c) concentration. It can be seen that the model-measurement agreement improves

473 significantly (model/obs closer to 1) after reducing NH_3 emissions for all three metrics. -3×NH₃_EMI would

474 reduce the mean NH_3, NH_4^+, and total NH_x concentration by ∼8.1 µg m⁻³, 3.2 µg m⁻³, and 11.3 µg m⁻³, respectively,

475 compared to the 3×Base HCl run. Even though reducing NH_3 emissions, it is still sufficient to react rapidly with

476 the varying HCl in the sensitivity experiments contributing to an increase in NH_4^+. As can be seen in Fig. 10b,

477 initially, NH_4^+ is somewhat lower, but it increases later and matches the 3×Base HCl run. This suggests that NH_4^+

478 formation in the model is more sensitive to changes in HCl than changes in NH_3 emission, while total NH_x agrees

479 well by reducing the NH_3 emissions. In general, CTMs have higher NH_3 concentration than observations, further

480 supporting models having too much NH_3. A few factors might contribute to the model discrepancies for NH_3:

481 there are uncertainties in the emission inventory of the bottom-up approach of NH_3, and the model does not

482 currently include the bidirectional exchange of NH_3 with surfaces, such as dew and fog water. Also model does

483 not have accurate industrial sources of HCl emission. Diurnal emission profiles are uncertainty for both NH_3 and

484 HCl. Furthermore, gas-to-particle partitioning associated with SO_2 oxidation pathways in the model is not correct

485 at present.

486 **4. Conclusions**

487 In this study, we have evaluated for the first time in South Asia the performance of a chemical transport model

488 (WRF-Chem) in modeling NH_3, NH_4^+, and total NH_x, by comparing against the WiFEX measurements

489 (MARGA). The model predicted average NH₃ and NH₄⁺ mass loadings of 56.7 ± 14.3 and 14.7 ± 4.9 µg m⁻³

490 respectively, whereas the measurements depicted 28.2 ± 12.4 and 36.9 ± 15.1 µg m⁻³, respectively, in the diurnal

491 concentration. Simulated NH₃ concentrations peaked with bimodal variation, though observations showed a

492 daytime rise around 12:00-13:00 h. Ammonia peaks during the daytime suggested that the NH₄⁺ volatilization is

493 causing its rise. Also, the role of fog and dew in enhancing NH₃ pulses requires further attention, and it is currently

494 not incorporated into the model. In daily means, we find NH_3 is significantly overestimated by the model, NH_4^+

495 was underestimated while simulated total NH_x agreed well with the measurement, indicating incorrect gas-to-

496 particle partitioning along with missing chemical process may impacts this mismatch in the model. The ability of

497 the model to accurately describe the gas-to-particle partitioning of the MARGA was evaluated by the fraction of

498 total NH_x (= NH_3 + NH_4^+) in the particulate phase (NH_4^+/NH_x). A strong relation of MARGA NH_4^+/NH_x was

499 observed with dominant anion (Cl⁻) (r = 0.79), whereas the standard model showed a strong correlation between

500 NH_4^+/NH_x with dominant anion (SO_4^{2-}) (r = 0.77), pointing to the missing chloride (HCl/Cl⁻) chemistry in the

501 model. Measured HCl/Cl⁻ correlated highly (r = 0.53) with the NH₄⁺ levels, in the presence high RH (70-100 %),

502 indicated HCl promoting the increase in the particle fraction of NH₄⁺ (49.5 %) with Cl⁻ (29.7 %) as the primary

503 ~~anion. On average, the measured aerosol neutralization ratio (ANR) was close to unity (0.96) with Cl⁻ the most~~

504 ~~significant anion followed by NO₃⁻ and SO₄²⁻.~~

505 We ~~further~~ incorporated HCl/Cl⁻ emissions in the model and conducted three sensitivity experiments of

506 varying HCl emissions, named as No HCl (0 mol km^{-2} h^{-1}), Base Case HCl (3× Sharma et al., 2019; 24.8 mol km^{-2}

507 h^{-1}) and 3×Base HCl (74 mol km^{-2} h^{-1}) run. The revised model shows that by adding HCl emissions ~~in the model~~

508 ~~were~~ more NH$_x$ was partition~~ed~~ing ~~more NH₃~~ to the condensed phase improving agreement with the observations,

509 ~~due to its high concentrations, reaching maximum mass loadings of NH₄⁺ and Cl⁻ of 70 and 110 μg m⁻³ μg m⁻³,~~

510 ~~respectively, in the 3×Base HCl run, while increasing the total mean NH_x concentration by 15 μg m⁻³ compared~~

511 ~~to the No HCl run.~~ 3×Base HCl was able to represent well the diurnal variation of NH₄⁺ and Cl⁻ both in terms of

512 amount and pattern with improved NMB for NH₃. Additional sensitivities tests in changing NH₃ emissions

513 (reduction by a factor of 3) in the 3×Base HCl also improved NH₃, NH₄⁺, and NH$_x$ concentrations. We find excess

514 NH₃ along with longer lifetime of NH₄⁺ may act as a controlling driver for NH$_x$ overestimation in the model.

515 These results highlight the need to include correct industrial sources of HCl emissions along with appropriate

516 emissions of NH₃ to reduce biases in NH$_x$.

517 ~~The NMB for NH₃ was found to be reduced from 1.38 to 1.13 while NMB for NH₄⁺ systematically~~

518 ~~improved from −0.61 to −0.03 in 3×Base HCl. By contrast, NMB for NH_x increased from 0.12 to 0.39, respectively,~~

519 ~~for the No HCl and 3×Base HCl simulations. Our modeling results suggest reducing NH₃ emissions by a factor~~

520 ~~of 3 (−3×NH₃_EMI) in the 3×Base HCl was successful in reducing the mean NH₃, NH₄⁺ and total NH_x~~

521 ~~concentration by ~ 8.1 μg m⁻³, 3.2 μg m⁻³, and 11.3 μg m⁻³, respectively, compared to the 3×Base HCl.~~ Developing

522 the appropriate NH₃ emissions using country-specific emission inventories, which are currently under

523 development as part of the Global Challenges Research Fund (GCRF), South Asian Nitrogen Hub (SANH). Also,

524 there is potential to develop top-down constraints on NH₃ emissions by taking inference from the satellite, model,

525 and ground-based observations. ~~We find excess NH₃ along with longer lifetime of NH₄⁺ may act as a controlling~~

526 ~~driver for NH_x overestimation in the model.~~ Challenges remain in simulating NH₃ as a contributor to particulate

527 matter due to temporal factors in ammonia peaks including the role of fog and dew where more work is needed.

528 This work also suggests model improvements to SO₂ oxidation pathways could improve NH$_x$ partitioning.

529 ~~Hence, in the future, it is necessary to evaluate the impact of the addition of correct industrial sources of~~

530 ~~HCl emission along with appropriate emissions of NH₃ and their diurnal variability, and improvements to the~~

531 ~~chemistry in model are suggested to address the challenges of simulating NH₃ as a contributor to particulate~~

532 ~~matter. Additionally, it is required to understand different SO₂ oxidation pathways in the model. To our~~

533 ~~knowledge, this is the first study to qualitatively examine the influence of HCl/Cl⁻ chemistry in WRF-Chem in~~

534 ~~determining the fraction of NH₄⁺/NH_x. The present study suggests that the bias in NH_x could be reduced by~~

535 ~~including both the accurate HCl and NH₃ emissions in the model. Developing the appropriate NH₃ emissions~~

536 ~~using country-specific emission inventories, which are currently under development as part of the Global~~

537 ~~Challenges Research Fund (GCRF), South Asian Nitrogen Hub (SANH). Also, there is potential to develop top-~~

538 ~~down constraints on NH₃ emissions by taking inference from the satellite, model, and ground-based observations.~~

Data availability

The $0.1° \times 0.1°$ emission grid maps can be downloaded from the EDGAR website on https://edgar.jrc.ec.europa.eu/htap_v2/index.php?SECURE=_123 per year per sector. Gridded emissions in t y^{-1} on a $0.1° \times 0.1°$ for HCl emissions can be downloaded from Mendeley data: http://dx.doi.org/10.17632/546t9249bv.1. The model data is available at Aditya, Indian Institute of Tropical Meteorology (IITM) super-computer and can be provided upon request to the corresponding author. The observational and meteorological data of WiFEX are available by contacting the corresponding author.

Author contributions

SDG designed the research; PVP performed the WRF-Chem model simulations and led the analysis; PA and RK contributed to data collection and its quality control and assurance; GG, RK, and PG helped with the model set up; PVP and SDG wrote the paper with contributions from all co-authors.

Competing interests

The authors declare that they have no conflict of interest.

Acknowledgments

We thank the Director, IITM, for his continuous support and encouragement. IITM is funded by the Ministry of Earth Sciences (MoES), Government of India. We wish to thank the MoES for supporting the WiFEX campaign. The lead author's fellowship was supported by the National Supercomputing Mission (NSM) program grant at C-DAC, and Ph.D. fees are covered by the Natural Environment Research Council (NERC) of UK Research and Innovation (UKRI)-Global Challenges Research Fund (GCRF), South Asian Nitrogen Hub (SANH), and we are grateful to the Executive Director and the Director-General of C-DAC and the SANH Director and Chair of the Executive Board. We acknowledge the availability of CPCB-NO_x, NO_2, and O_3 data from the CPCB web portal (https://app.cpcbccr.com/ccr, last access: 1 December 2021). We wish to acknowledge the National Center for Atmospheric Research is sponsored by the National Science Foundation.

5. References

Acharja, P., Ali, K., Trivedi, D. K., Safai, P. D., Ghude, S., Prabhakaran, T. and Rajeevan, M.: Characterization of atmospheric trace gases and water soluble inorganic chemical ions of PM1 and PM2.5 at Indira Gandhi International Airport, New Delhi during 2017–18 winter, Sci. Total Environ., 729, 138800, doi:10.1016/j.scitotenv.2020.138800, 2020.

Acharja, P., Ali, K., Ghude, S. D., Sinha, V., Sinha, B., Kulkarni, R., Gultepe, I. and Nair, M.: Chemosphere Enhanced secondary aerosol formation driven by excess ammonia during fog episodes, Chemosphere, 289(November 2021), 133155, doi:10.1016/j.chemosphere.2021.133155, 2021.

Ali, K., Acharja, P., Trivedi, D. K., Kulkarni, R., Pithani, P., Safai, P. D., Chate, D. M., Ghude, S., Jenamani, R.

K. and Rajeevan, M.: Characterization and source identification of PM 2.5 and its chemical and carbonaceous constituents during Winter Fog Experiment 2015–16 at Indira Gandhi International Airport, Delhi, Sci. Total Environ., 662, 687–696, doi:10.1016/j.scitotenv.2019.01.285, 2019.

Aneja, V. P., Murray, G. C. and Southerland, J.: Atmospheric nitrogen compounds: Emissions, transport, transformation, deposition, and assessment, EM Air Waste Manag. Assoc. Mag. Environ. Manag., 22–25, 1998.

Behera, S. N., Sharma, M., Aneja, V. P. and Balasubramanian, R.: Ammonia in the atmosphere: a review on emission sources, atmospheric chemistry and deposition on terrestrial bodies, Environ. Sci. Pollut. Res., 20(11), 8092–8131, doi:10.1007/s11356-013-2051-9, 2013.

Bucaram, C. J. and Bowman, F. M.: Wrf-chem modeling of summertime air pollution in the northern great plains: Chemistry and aerosol mechanism intercomparison, Atmosphere (Basel)., 12(9), doi:10.3390/atmos12091121, 2021.

Carslaw, D. C. and Ropkins, K.: Openair - An r package for air quality data analysis, Environ. Model. Softw., 27–28(July 2019), 52–61, doi:10.1016/j.envsoft.2011.09.008, 2012.

Chaudhary, P., Garg, S., George, T., Shabin, M., Saha, S., Subodh, S. and Sinha, B.: Underreporting and open burning – the two largest challenges for sustainable waste management in India, Resour. Conserv. Recycl., 175, 105865, doi:https://doi.org/10.1016/j.resconrec.2021.105865, 2021.

Chen, Y., Wang, Y., Nenes, A., Wild, O., Song, S., Hu, D., Liu, D., He, J., Hildebrandt Ruiz, L., Apte, J. S., Gunthe, S. S. and Liu, P.: Ammonium Chloride Associated Aerosol Liquid Water Enhances Haze in Delhi, India, Environ. Sci. Technol., 56(11), 7163–7173, doi:10.1021/acs.est.2c00650, 2022.

Clarisse, L., Clerbaux, C., Dentener, F., Hurtmans, D. and Coheur, P. F.: Global ammonia distribution derived from infrared satellite observations, Nat. Geosci., 2(7), 479–483, doi:10.1038/ngeo551, 2009.

Clarisse, L., Shephard, M. W., Dentener, F., Hurtmans, D., Cady-Pereira, K., Karagulian, F., Van Damme, M., Clerbaux, C. and Coheur, P. F.: Satellite monitoring of ammonia: A case study of the San Joaquin Valley, J. Geophys. Res. Atmos., 115(13), 1–15, doi:10.1029/2009JD013291, 2010.

CPCB: Annual Report 2014-15., 2014.

CPCB: Annual Report Annual Report., 2020.

Van Damme, M., Clarisse, L., Whitburn, S., Hadji-Lazaro, J., Hurtmans, D., Clerbaux, C. and Coheur, P. F.: Industrial and agricultural ammonia point sources exposed, Nature, 564(7734), 99–103, doi:10.1038/s41586-018-0747-1, 2018.

Datta, A., Sharma, S. K., Harit, R. C., Kumar, V., Mandal, T. K. and Pathak, H.: Ammonia emission from subtropical crop land area in india, Asia-Pacific J. Atmos. Sci., 48(3), 275–281, doi:10.1007/s13143-012-0027-1, 2012.

Duan, X., Yan, Y., Peng, L., Xie, K., Hu, D., Li, R. and Wang, C.: Role of ammonia in secondary inorganic aerosols formation at an ammonia-rich city in winter in north China: A comparative study among industry, urban, and rural sites, Environ. Pollut., 291(May), 118151, doi:10.1016/j.envpol.2021.118151, 2021.

Ellis, R. A., Murphy, J. G., Markovic, M. Z., Vandenboer, T. C., Makar, P. A., Brook, J. and Mihele, C.: The influence of gas-particle partitioning and surface-atmosphere exchange on ammonia during BAQS-Met, Atmos. Chem. Phys., 11(1), 133–145, doi:10.5194/acp-11-133-2011, 2011.

FINNv1.5: FINN Data, [online] Available from: http://bai.acom.ucar.edu/Data/fire/ (Accessed 15 April 2019), n.d.

611 Freitas, S. R., Longo, K. M., Chatfield, R., Latham, D., Silva Dias, M. A. F., Andreae, M. O., Prins, E., Santos, J.
612 C., Gielow, R. and Carvalho Jr., J. A.: Including the sub-grid scale plume rise of vegetation fires in low resolution
613 atmospheric transport models, Atmos. Chem. Phys., 7(13), 3385–3398, doi:10.5194/acp-7-3385-2007, 2007.

614 Georgiou, G. K., Christoudias, T., Proestos, Y., Kushta, J., Hadjinicolaou, P. and Lelieveld, J.: Air quality
615 modelling in the summer over the eastern Mediterranean using WRF-Chem: chemistry and aerosol mechanism
616 intercomparison, Atmos. Chem. Phys., 18(3), 1555–1571, doi:10.5194/acp-18-1555-2018, 2018.

617 Ghude, S., Kumar, R., Jena, C., Debnath, S., Kulkarni, R., Alessandrini, S., Biswas, M., Kulkrani, S., Pithani, P.,
618 Kelkar, S., Sajjan, V., Chate, D., Soni, V., Singh, S., Nanjundiah, R. and Rajeevan, M.: Evaluation of PM2.5
619 Forecast using Chemical Data Assimilation in the WRF-Chem Model: A Novel Initiative Under the Ministry of
620 Earth   Sciences   Air   Quality   Early   Warning   System   for   Delhi,   India,   Curr.   Sci.,   118,
621 doi:10.18520/cs/v118/i11/1803-1815, 2020.

622 Ghude, S. D.: Premature mortality in India due to PM2.5 and ozone exposure, Geophys. Res. Lett., 1–8,
623 doi:10.1002/2013GL058740.Received, 2016.

624 Ghude, S. D., Fadnavis, S., Beig, G., Polade, S. D. and van der A, R. J.: Detection of surface emission hot spots,
625 trends, and seasonal cycle from satellite-retrieved NO $_2$ over India, J. Geophys. Res., 113(D20), D20305,
626 doi:10.1029/2007JD009615, 2008a.

627 Ghude, S. D., Jain, S. L., Arya, B. C., Beig, G., Ahammed, Y. N., Kumar, A. and Tyagi, B.: Ozone in ambient air
628 at a tropical megacity, Delhi: Characteristics, trends and cumulative ozone exposure indices, J. Atmos. Chem.,
629 60(3), 237–252, doi:10.1007/s10874-009-9119-4, 2008b.

630 Ghude, S. D., Van der A, R. J., Beig, G., Fadnavis, S. and Polade, S. D.: Satellite derived trends in NO2 over the
631 major global hotspot regions during the past decade and their inter-comparison, Environ. Pollut., 157(6), 1873–
632 1878, doi:10.1016/j.envpol.2009.01.013, 2009.

633 Ghude, S. D., Lal, D. M., Beig, G., van der A, R. and Sable, D.: Rain-Induced Soil NO $_x$ Emission From India
634 During the Onset of the Summer Monsoon: A Satellite Perspective, J. Geophys. Res., 115(D16), D16304,
635 doi:10.1029/2009JD013367, 2010.

636 Ghude, S. D., Pfister, G. G., Jena, C. K., Emmons, L. K., Kumar, R. and van der A, R. J.: Satellite constraints of
637 Nitrogen Oxide (NOX) emissions from India based on OMI observations and WRF-Chem simulations, Geophys.
638 Res. Lett., 40(x), 423–428, doi:10.1029/2012gl053926, 2012.

639 Ghude, S. D., Kulkarni, S. H., Jena, C., Pfister, G. G., Beig, G., Fadnavis, S. and Van Der, R. J.: Application of
640 satellite observations for identifying regions of dominant sources of nitrogen oxides over the indian subcontinent,
641 J. Geophys. Res. Atmos., 118(2), 1075–1089, doi:10.1029/2012JD017811, 2013.

642 Ghude, S. D., Bhat, G. S., Prabhakaran, T., Jenamani, R. K., Chate, D. M., Safai, P. D., Karipot, A. K., Konwar,
643 M., Pithani, P., Sinha, V., Rao, P. S. P., Dixit, S. A., Tiwari, S., Todekar, K., Varpe, S., Srivastava, A. K., Bisht,
644 D. S., Murugavel, P., Ali, K., Mina, U., Dharua, M., Rao, Y. J., Padmakumari, B., Hazra, A., Nigam, N., Shende,
645 U., Lal, D. M., Chandra, B. P., Mishra, A. K., Kumar, A., Hakkim, H., Pawar, H., Acharja, P., Kulkarni, R.,
646 Subharthi, C., Balaji, B., Varghese, M., Bera, S. and Rajeevan, M.: Winter fog experiment over the Indo-Gangetic
647 plains of India, Curr. Sci., 112(4), doi:10.18520/cs/v112/i04/767-784, 2017.

648 Ghude, S. D., Kumar, R., Govardhan, G., Jena, C., Nanjundiah, R. S. and Rajeevan, M.: New Delhi: air-quality
649 warning system cuts peak pollution, Nature, 602(7896), 211, doi:10.1038/D41586-022-00332-Y, 2022.

650 Ginoux, P., Chin, M., Tegen, I., Goddard, T. and In-, G.: Sources and distribution of dust aerosols simulated with

651   the GOCART model, J. Geophys. Res., 106, 20255–20273, doi:https://doi.org/10.1029/2000JD000053, 2001.

652   Gu, B., Zhang, L., Dingenen, R. Van, Vieno, M., Grinsven, H. J. Van, Zhang, X., Zhang, S., Chen, Y., Wang, S.,

653   Ren, C., Rao, S., Holland, M., Winiwarter, W., Chen, D., Xu, J. and Sutton, M. A.: Abating ammonia is more

654   cost-effective than nitrogen oxides for mitigating PM2.5 air pollution, Science (80-.)., 374(6568), 758–762,

655   doi:10.1126/science.abf8623, 2021.

656   Guenther, A., Karl, T., Harley, P., Wiedinmyer, C., Palmer, P. I. and Geron, C.: Estimates of global terrestrial

657   isoprene emissions using MEGAN (Model of Emissions of Gases and Aerosols from Nature), Atmos. Chem.

658   Phys., 6(11), 3181–3210, doi:10.5194/acp-6-3181-2006, 2006.

659   Gunthe, S. S., Liu, P., Panda, U., Raj, S. S., Sharma, A., Darbyshire, E., Reyes-Villegas, E., Allan, J., Chen, Y.,

660   Wang, X., Song, S., Pöhlker, M. L., Shi, L., Wang, Y., Kommula, S. M., Liu, T., Ravikrishna, R., McFiggans, G.,

661   Mickley, L. J., Martin, S. T., Pöschl, U., Andreae, M. O. and Coe, H.: Enhanced aerosol particle growth sustained

662   by high continental chlorine emission in India, Nat. Geosci., 14(2), 77–84, doi:10.1038/s41561-020-00677-x,

663   2021.

664   Gupta, M. and Mohan, M.: Validation of WRF/Chem model and sensitivity of chemical mechanisms to ozone

665   simulation over megacity Delhi, Atmos. Environ., 122, 220–229, doi:10.1016/j.atmosenv.2015.09.039, 2015.

666   Hindustan Times: 66 dairies, six dyeing units shut down in east Delhi, Hindustan Times, 6th July, 2021.

667   Hristov, A. N., Hanigan, M., Cole, A., Todd, R., McAllister, T. A., Ndegwa, P. M. and Rotz, A.: Review:

668   Ammonia emissions from dairy farms and beef feedlots, Can. J. Anim. Sci., 91(1), 1–35, doi:10.4141/CJAS10034,

669   2011.

670   Huang, X., Song, Y., Li, M., Li, J., Huo, Q., Cai, X., Zhu, T., Hu, M. and Zhang, H.: A high-resolution ammonia

671   emission inventory in China, Global Biogeochem. Cycles, 26(1), 1–14, doi:10.1029/2011GB004161, 2012.

672   Ianniello, A., Spataro, F., Esposito, G., Allegrini, I., Rantica, E., Ancora, M. P., Hu, M. and Zhu, T.: Occurrence

673   of gas phase ammonia in the area of Beijing (China), Atmos. Chem. Phys., 10(19), 9487–9503, doi:10.5194/acp-

674   10-9487-2010, 2010.

675   Ianniello, A., Spataro, F., Esposito, G., Allegrini, I., Hu, M. and Zhu, T.: Chemical characteristics of inorganic

676   ammonium salts in PM2.5 in the atmosphere of Beijing (China), Atmos. Chem. Phys., 11(21), 10803–10822,

677   doi:10.5194/acp-11-10803-2011, 2011.

678   Jaiprakash, Singhai, A., Habib, G., Raman, R. S. and Gupta, T.: Chemical characterization of PM1.0 aerosol in

679   Delhi and source apportionment using positive matrix factorization, Environ. Sci. Pollut. Res., 24(1), 445–462,

680   doi:10.1007/s11356-016-7708-8, 2017.

681   Jena, C., Ghude, S., Kulkarni, R., Debnath, S., Kumar, R., Soni, V. K., Acharja, P., Kulkarni, S., Khare, M.,

682   Kaginalkar, A., Chate, D., Ali, K., Nanjundiah, R. and Rajeevan, M.: Evaluating the sensitivity of fine particulate

683   matter (PM$_{2.5}$) simulations to chemical mechanism in Delhi, Atmos. Chem. Phys.

684   Discuss., (3), 1–28, doi:10.5194/acp-2020-673, 2020.

685   Jena, C., Ghude, S. D., Kumar, R., Debnath, S., Govardhan, G., Soni, V. K., Kulkarni, S. H., Beig, G., Nanjundiah,

686   R. S. and Rajeevan, M.: Performance of high resolution (400 m) PM2.5 forecast over Delhi, Sci. Rep., 11(1), 1–

687   9, doi:10.1038/s41598-021-83467-8, 2021.

688   Knote, C., Hodzic, A. and Jimenez, J. L.: The effect of dry and wet deposition of condensable vapors on secondary

689   organic aerosols concentrations over the continental US, Atmos. Chem. Phys., 15(1), 1–18, doi:10.5194/acp-15-

690   1-2015, 2015.

691 Kulkarni, S. H., Ghude, S. D., Jena, C., Karumuri, R. K., Sinha, B., Sinha, V., Kumar, R., Soni, V. K. and Khare,
692 M.: How Much Does Large-Scale Crop Residue Burning Affect the Air Quality in Delhi?, Environ. Sci. Technol.,
693 54(8), 4790–4799, doi:10.1021/acs.est.0c00329, 2020.

694 Kumar, A., Hakkim, H., Ghude, S. D. and Sinha, V.: Probing wintertime air pollution sources in the Indo-Gangetic
695 Plain through 52 hydrocarbons measured rarely at Delhi & Mohali, Sci. Total Environ., 801, 149711,
696 doi:https://doi.org/10.1016/j.scitotenv.2021.149711, 2021.

697 Kumar, R., Barth, M. C., Pfister, G. G., Delle Monache, L., Lamarque, J. F., Archer-Nicholls, S., Tilmes, S.,
698 Ghude, S. D., Wiedinmyer, C., Naja, M. and Walters, S.: How Will Air Quality Change in South Asia by 2050?,
699 J. Geophys. Res. Atmos., 123(3), 1840–1864, doi:10.1002/2017JD027357, 2018.

700 Kumar, R., Ghude, S. D., Biswas, M., Jena, C., Alessandrini, S., Debnath, S., Kulkarni, S., Sperati, S., Soni, V.
701 K., Nanjundiah, R. S. and Rajeevan, M.: Enhancing Accuracy of Air Quality and Temperature Forecasts During
702 Paddy Crop Residue Burning Season in Delhi Via Chemical Data Assimilation, J. Geophys. Res. Atmos., 125(17),
703 1–16, doi:10.1029/2020JD033019, 2020.

704 Kuttippurath, J., Singh, A., Dash, S. P., Mallick, N., Clerbaux, C., Van Damme, M., Clarisse, L., Coheur, P. F.,
705 Raj, S., Abbhishek, K. and Varikoden, H.: Record high levels of atmospheric ammonia over India: Spatial and
706 temporal analyses, Sci. Total Environ., 740, 139986, doi:10.1016/j.scitotenv.2020.139986, 2020.

707 Lan, Z., Lin, W., Pu, W. and Ma, Z.: Measurement report: Exploring NH3behavior in urban and suburban Beijing:
708 Comparison and implications, Atmos. Chem. Phys., 21(6), 4561–4573, doi:10.5194/acp-21-4561-2021, 2021.

709 Laubach, J., Taghizadeh-Toosi, A., Gibbs, S. J., Sherlock, R. R., Kelliher, F. M. and Grover, S. P. P.: Ammonia
710 emissions from cattle urine and dung excreted on pasture, Biogeosciences, 10(1), 327–338, doi:10.5194/bg-10-
711 327-2013, 2013.

712 Leytem, A. B., Bjorneberg, D. L., Rotz, C. A., Moraes, L. E., Kebreab, E. and Dungan, R. S.: Ammonia emissions
713 from dairy lagoons in the western U.S., Trans. ASABE, 61(3), 1001–1015, doi:10.13031/trans.12646, 2018.

714 Li, L., Chen, Z. M., Zhang, Y. H., Zhu, T., Li, S., Li, H. J., Zhu, L. H. and Xu, B. Y.: Heterogeneous oxidation of
715 sulfur dioxide by ozone on the surface of sodium chloride and its mixtures with other components, J. Geophys.
716 Res. Atmos., 112(18), 1–13, doi:10.1029/2006JD008207, 2007.

717 Makkonen, U., Virkkula, A., Mäntykenttä, J., Hakola, H., Keronen, P., Vakkari, V. and Aalto, P. P.: Semi-
718 continuous gas and inorganic aerosol measurements at a Finnish urban site: comparisons with filters, nitrogen in
719 aerosol and gas phases, and aerosol acidity, Atmos. Chem. Phys., 12(12), 5617–5631, doi:10.5194/acp-12-5617-
720 2012, 2012.

721 Mandal, T. K., Saxena, M., Rohtash, Sharma, S. K., Gupta, N. C., Kumar, M. and Saraswati: Characteristics of
722 ambient ammonia over Delhi, India, Meteorol. Atmos. Phys., 124(1–2), 67–82, doi:10.1007/s00703-013-0299-8,
723 2013.

724 Meng, Z., Xu, X., Lin, W., Ge, B., Xie, Y., Song, B., Jia, S., Zhang, R., Peng, W., Wang, Y., Cheng, H., Yang,
725 W. and Zhao, H.: Role of ambient ammonia in particulate ammonium formation at a rural site in the North China
726 Plain, Atmos. Chem. Phys., 18(1), 167–184, doi:10.5194/acp-18-167-2018, 2018.

727 Metzger, S., Mihalopoulos, N. and Lelieveld, J.: Importance of mineral cations and organics in gas-aerosol
728 partitioning of reactive nitrogen compounds: Case study based on MINOS results, Atmos. Chem. Phys., 6(9),
729 2549–2567, doi:10.5194/acp-6-2549-2006, 2006.

730 Móring, A., Hooda, S., Raghuram, N., Adhya, T. K., Ahmad, A., Bandyopadhyay, S. K., Barsby, T., Beig, G.,

Bentley, A. R., Bhatia, A., Dragosits, U., Drewer, J., Foulkes, J., Ghude, S. D., Gupta, R., Jain, N., Kumar, D., Kumar, R. M., Ladha, J. K., Mandal, P. K., Neeraja, C. N., Pandey, R., Pathak, H., Pawar, P., Pellny, T. K., Poole, P., Price, A., Rao, D. L. N., Reay, D. S., Singh, N. K., Sinha, S. K., Srivastava, R. K., Shewry, P., Smith, J., Steadman, C. E., Subrahmanyam, D., Surekha, K., Venkatesh, K., Varinderpal-Singh, Uwizeye, A., Vieno, M. and Sutton, M. A.: Nitrogen Challenges and Opportunities for Agricultural and Environmental Science in India, Front. Sustain. Food Syst., 5, 13, doi:10.3389/fsufs.2021.505347, 2021.

Nair, A. A. and Yu, F.: Quantification of atmospheric ammonia concentrations: A review of its measurement and modeling, Atmosphere (Basel)., 11(10), doi:10.3390/atmos11101092, 2020.

Nenes, A., Pandis, S. N., Weber, R. J. and Russell, A.: Aerosol pH and liquid water content determine when particulate matter is sensitive to ammonia and nitrate availability, Atmos. Chem. Phys., 20(5), 3249–3258, doi:10.5194/acp-20-3249-2020, 2020.

NIVDANGE, S., Jena, C. and Pawar, P.: Nationwide CoViD-19 lockdown impact on air quality in India, MAUSAM, 73(1), 115–128, doi:10.54302/mausam.v73i1.1475, 2022.

Pawar, P. V., Ghude, S. D., Jena, C., Móring, A., Sutton, M. A., Kulkarni, S., Lal, D. M., Surendran, D., Van Damme, M., Clarisse, L., Coheur, P.-F., Liu, X., Govardhan, G., Xu, W., Jiang, J. and Adhya, T. K.: Analysis of atmospheric ammonia over South and East Asia based on the MOZART-4 model and its comparison with satellite and surface observations, Atmos. Chem. Phys., 21(8), 6389–6409, doi:10.5194/acp-21-6389-2021, 2021.

Pinder, R. W., Adams, P. J. and Pandis, S. N.: Ammonia Emission Controls as a Cost-Effective Strategy for Reducing Atmospheric Particulate Matter in the Eastern United States, Environ. Sci. Technol., 41(2), 380–386, doi:10.1021/es060379a, 2007.

Pinder, R. W., Gilliland, A. B. and Dennis, R. L.: Environmental impact of atmospheric NH3 emissions under present and future conditions in the eastern United States, Geophys. Res. Lett., 35(12), doi:10.1029/2008GL033732, 2008.

Pollution, C. and Board, C.: Guidelines for Manual Sampling & Analyses., 2011.

Saraswati, George, M. P., Sharma, S. K., Mandal, T. K. and Kotnala, R. K.: Simultaneous Measurements of Ambient NH 3 and Its Relationship with Other Trace Gases, PM 2.5 and Meteorological Parameters over Delhi, India, Mapan - J. Metrol. Soc. India, 34(1), 55–69, doi:10.1007/s12647-018-0286-0, 2019.

Seinfeld, J. H. and Pandis, S. N.: Atmospheric chemistry and physics : from air pollution to climate change., n.d.

Seinfeld, J. H., Bretherton, C., Carslaw, K. S., Coe, H., DeMott, P. J., Dunlea, E. J., Feingold, G., Ghan, S., Guenther, A. B., Kahn, R., Kraucunas, I., Kreidenweis, S. M., Molina, M. J., Nenes, A., Penner, J. E., Prather, K. A., Ramanathan, V., Ramaswamy, V., Rasch, P. J., Ravishankara, A. R., Rosenfeld, D., Stephens, G. and Wood, R.: Improving our fundamental understanding of the role of aerosol–cloud interactions in the climate system, Proc. Natl. Acad. Sci. U. S. A., 113(21), 5781, 2016.

Sha, T., Ma, X., Jia, H., Tian, R., Chang, Y., Cao, F. and Zhang, Y.: Aerosol chemical component: Simulations with WRF-Chem and comparison with observations in Nanjing, Atmos. Environ., 218(June), 116982, doi:10.1016/j.atmosenv.2019.116982, 2019.

Sharma, C., Tiwari, M. K. and Pathak, H.: Estimates of emission and deposition of reactive nitrogenous species for India, Curr. Sci., 94(11), 1439–1446, 2008.

Sharma, G., Sinha, B., Pallavi, Hakkim, H., Chandra, B. P., Kumar, A. and Sinha, V.: Gridded Emissions of CO, NOx, SO2, CO2, NH3, HCl, CH4, PM2.5, PM10, BC, and NMVOC from Open Municipal Waste Burning in

771   India, Environ. Sci. Technol., 53(9), 4765–4774, doi:10.1021/acs.est.8b07076, 2019.

772   Sharma, S. K., Saxena, M., Saud, T., Korpole, S. and Mandal, T. K.: Measurement of NH3, NO, NO2 and related

773   particulates at urban sites of indo gangetic plain (IGP) of India, J. Sci. Ind. Res. (India)., 71(5), 360–362, 2012.

774   Sharma, S. K., Harit, R. C., Kumar, V., Mandal, T. K. and Pathak, H.: Ammonia Emission from Rice-Wheat

775   Cropping System in Subtropical Soil of India, Agric. Res., 3(2), 175–180, doi:10.1007/s40003-014-0107-9,

776   2014a.

777   Sharma, S. K., Kumar, M., Rohtash, Gupta, N. C., Saraswati, Saxena, M. and Mandal, T. K.: Characteristics of

778   ambient ammonia over Delhi, India., 2014b.

779   Sharma, S. K., Kotnala, G. and Mandal, T. K.: Spatial Variability and Sources of Atmospheric Ammonia in India:

780   A Review, Aerosol Sci. Eng., 4(1), doi:10.1007/s41810-019-00052-3, 2020.

781   Sherlock, R. R., Freney, J. R., Bacon, P. E. and van der Weerden, T. J.: Estimating ammonia volatilization from

782   unsaturated urea fertilized and urine affected soils by an indirect method, Fertil. Res., 40(3), 197–205,

783   doi:10.1007/BF00750466, 1994.

784   Singh, G. K., Rajeev, P., Paul, D. and Gupta, T.: Chemical characterization and stable nitrogen isotope

785   composition of nitrogenous component of ambient aerosols from Kanpur in the Indo-Gangetic Plains., Sci. Total

786   Environ., 763, 143032, doi:10.1016/j.scitotenv.2020.143032, 2021.

787   Stieger, B., Spindler, G., van Pinxteren, D., Grüner, A., Wallasch, M. and Herrmann, H.: Development of an

788   online-coupled MARGA upgrade for the 2\,h interval quantification of low-molecular-weight organic acids in the

789   gas and particle phases, Atmos. Meas. Tech., 12(1), 281–298, doi:10.5194/amt-12-281-2019, 2019.

790   Sutton, M. A. and Howard, C. M.: Ammonia maps make history, Nature, 564(7734), 49–50, 2018.

791   Sutton, M. A., Burkhardt, J. K., Guerin, D., Nemitz, E. and Fowler, D.: Development of resistance models to

792   describe measurements of bi-directional ammonia surface-atmosphere exchange, Atmos. Environ., 32(3), 473–

793   480, doi:10.1016/S1352-2310(97)00164-7, 1998.

794   Sutton, M. A., Erisman, J. W., Dentener, F. and Möller, D.: Ammonia in the environment: From ancient times to

795   the present, Environ. Pollut., 156(3), 583–604, doi:10.1016/j.envpol.2008.03.013, 2008.

796   Sutton, M. A., Reis, S. and Baker, S. M. H.: Atmospheric Ammonia: Detecting emission changes and

797   environmental impacts., 2009a.

798   Sutton, M. A., Nemitz, E., Milford, C., Campbell, C., Erisman, J. W., Hensen, A., Cellier, P., David, M., Loubet,

799   B., Personne, E., Schjoerring, J. K., Mattsson, M., Dorsey, J. R., Gallagher, M. W., Horvath, L., Weidinger, T.,

800   Meszaros, R., Dämmgen, U., Neftel, A., Herrmann, B., Lehman, B. E., Flechard, C. and Burkhardt, J.: Dynamics

801   of ammonia exchange with cut grassland: synthesis of results and conclusions of the GRAMINAE Integrated

802   Experiment, Biogeosciences, 6(12), 2907–2934, doi:10.5194/bg-6-2907-2009, 2009b.

803   Sutton, M. A., Reis, S., Riddick, S. N., Dragosits, U., Nemitz, E., Theobald, M. R., Tang, Y. S., Braban, C. F.,

804   Vieno, M., Dore, A. J., Mitchell, R. F., Wanless, S., Daunt, F., Fowler, D., Blackall, T. D., Milford, C., Flechard,

805   C. R., Loubet, B., Massad, R., Cellier, P., Personne, E., Coheur, P. F., Clarisse, L., Van Damme, M., Ngadi, Y.,

806   Clerbaux, C., Skjøth, C. A., Geels, C., Hertel, O., Kruit, R. J. W., Pinder, R. W., Bash, J. O., Walker, J. T.,

807   Simpson, D., Horváth, L., Misselbrook, T. H., Bleeker, A., Dentener, F. and de Vries, W.: Towards a climate-

808   dependent paradigm of ammonia emission and deposition, Philos. Trans. R. Soc. B Biol. Sci., 368(1621),

809   20130166–20130166, doi:10.1098/rstb.2013.0166, 2013.

810   Sutton, M. A., Drewer, J., Moring, A., Adhya, T. K., Ahmed, A., Bhatia, A., Brownlie, W., Dragosits, U., Ghude,

811   S. D., Hillier, J., Hooda, S., Howard, C. M., Jain, N., Kumar, D., Kumar, R. M., Nayak, D. R., Neeraja, C. N.,

812   Prasanna, R., Price, A., Ramakrishnan, B., Reay, D. S., Singh, R., Skiba, U., Smith, J. U., Sohi, S., Subrahmanyan,

813   D., Surekha, K., van Grinsven, H. J. M., Vieno, M., Voleti, S. R., Pathak, H. and Raghuram, N.: 2 - The Indian

814   Nitrogen Challenge in a Global Perspective, in The Indian Nitrogen Assessment, edited by Y. P. Abrol, T. K.

815   Adhya, V. P. Aneja, N. Raghuram, H. Pathak, U. Kulshrestha, C. Sharma, and B. Singh, pp. 9–28, Elsevier.,

816   2017a.

817   Sutton, M. A., J. Drewer, A. Moring, T.K Adhya, A. Ahmed and A. Bhatia: The Indian nitrogen assessment :

818   sources of reactive nitrogen, environmental and climate effects, management options, and policies, in The Indian

819   Nitrogen Assessment, edited by Y. P. Abrol, T. K. Adhya, V. P. Aneja, N. Raghuram, H. Pathak, U. Kulshrestha,

820   C. Sharma, and B. Singh, pp. 9–25, Elsevier., 2017b.

821   Sutton, M. A., Van Dijk, N., Levy, P. E., Jones, M. R., Leith, I. D., Sheppard, L. J., Leeson, S., Sim Tang, Y.,

822   Stephens, A., Braban, C. F., Dragosits, U., Howard, C. M., Vieno, M., Fowler, D., Corbett, P., Naikoo, M. I.,

823   Munzi, S., Ellis, C. J., Chatterjee, S., Steadman, C. E., Móring, A. and Wolseley, P. A.: Alkaline air: changing

824   perspectives on nitrogen and air pollution in an ammonia-rich world: Alkaline Air, Philos. Trans. R. Soc. A Math.

825   Phys. Eng. Sci., 378(2183), doi:10.1098/rsta.2019.0315, 2020.

826   Technical specifications for CAAQM station: TECHNICAL SPECIFICATIONS FOR CONTINUOUS

827   AMBIENT AIR QUALITY MONITORING (CAAQM) STATION (REAL TIME) Central Pollution Control

828   Board East Arjun Nagar , Shahdara., 2019.

829   Thomas, R. M., Trebs, I., Otjes, R., Jongejan, P. A. C., Brink, H. ten, Phillips, G., Kortner, M., Meixner, F. X.

830   and Nemitz, E.: An Automated Analyzer to Measure Surface-Atmosphere Exchange Fluxes of Water Soluble

831   Inorganic Aerosol Compounds and Reactive Trace Gases, Environ. Sci. \& Technol., 43(5), 1412–1418,

832   doi:10.1021/es8019403, 2009.

833   Twigg, M. M., Di Marco, C. F., Leeson, S., van Dijk, N., Jones, M. R., Leith, I. D., Morrison, E., Coyle, M.,

834   Proost, R., Peeters, A. N. M., Lemon, E., Frelink, T., Braban, C. F., Nemitz, E. and Cape, J. N.: Water soluble

835   aerosols and gases at a UK background site – Part 1: Controls of $PM_{2.5}$ and PM_{10} aerosol

836   composition, Atmos. Chem. Phys., 15(14), 8131–8145, doi:10.5194/acp-15-8131-2015, 2015.

837   Wagh, S., Singh, P., Ghude, S. D., Safai, P., Prabhakaran, T. and Kumar, P. P.: Study of ice nucleating particles

838   in fog-haze weather at New Delhi, India: A case of polluted environment, Atmos. Res., 259, 105693,

839   doi:https://doi.org/10.1016/j.atmosres.2021.105693, 2021.

840   Wang, Q., Miao, Y. and Wang, L.: Regional transport increases ammonia concentration in Beijing, China,

841   Atmosphere (Basel)., 11(6), doi:10.3390/ATMOS11060563, 2020a.

842   Wang, S., Nan, J., Shi, C., Fu, Q., Gao, S., Wang, D., Cui, H., Saiz-Lopez, A. and Zhou, B.: Atmospheric ammonia

843   and its impacts on regional air quality over the megacity of Shanghai, China, Sci. Rep., 5(October), 1–13,

844   doi:10.1038/srep15842, 2015.

845   Wang, T., Song, Y., Xu, Z., Liu, M., Xu, T., Liao, W., Yin, L., Cai, X., Kang, L., Zhang, H. and Zhu, T.: Why is

846   the Indo-Gangetic Plain the region with the largest NH3column in the globe during pre-monsoon and monsoon

847   seasons?, Atmos. Chem. Phys., 20(14), 8727–8736, doi:10.5194/acp-20-8727-2020, 2020b.

848   Warner, J. X., Dickerson, R. R., Wei, Z., Strow, L. L., Wang, Y. and Liang, Q.: Increased atmospheric ammonia

849   over the world's major agricultural areas detected from space, Geophys. Res. Lett., 44(6), 2875–2884,

850   doi:10.1002/2016GL072305, 2017.

851 Wentworth, G. R., Murphy, J. G., Gregoire, P. K., Cheyne, C. A. L., Tevlin, A. G. and Hems, R.: Soil-atmosphere
852 exchange of ammonia in a non-fertilized grassland: Measured emission potentials and inferred fluxes,
853 Biogeosciences, 11(20), 5675–5686, doi:10.5194/bg-11-5675-2014, 2014.

854 Wentworth, G. R., Murphy, J. G., Benedict, K. B., Bangs, E. J. and Collett, J. L.: The role of dew as a night-time
855 reservoir and morning source for atmospheric ammonia, Atmos. Chem. Phys., 16(11), 7435–7449,
856 doi:10.5194/acp-16-7435-2016, 2016.

857 Xu, J., Chen, J., Huo, J., Lin, Y., Fu, Q., Guo, H. and Lee, S. H.: Importance of gas-particle partitioning of
858 ammonia in haze formation in the rural agricultural environment, Atmos. Chem. Phys., 20(12), 7259–7269,
859 doi:10.5194/acp-20-7259-2020, 2020.

860 Yang, J., Kang, S. and Ji, Z.: Sensitivity analysis of chemical mechanisms in the WRF-chem model in
861 reconstructing aerosol concentrations and optical properties in the Tibetan Plateau, Aerosol Air Qual. Res., 18(2),
862 505–521, doi:10.4209/aaqr.2017.05.0156, 2018.

863 Zhang, X., Liu, J., Han, H., Zhang, Y., Jiang, Z., Wang, H., Meng, L., Li, Y. C. and Liu, Y.: Satellite-Observed
864 Variations and Trends in Carbon Monoxide over Asia and Their Sensitivities to Biomass Burning, Remote Sens.,
865 12(5), 830, doi:10.3390/rs12050830, 2020.

866
867
868
869
870
871
872
873
874
875
876
877
878
879
880
881
882
883
884
885
886
887

    FIGURE CAPTIONS

889   **Figure 1. (a) Comparison of observed and simulated average diurnal variation in (a) meteorological**
890   **parameters such as Temperature (T in °c) and Relative humidity (RH in %) and (b) NH$_3$ and NH$_4^+$**
891   **concentration (μg m^{-3}) during the sampling period (bar indicates mean standard deviation of each hour).**
892
893   **Figure 2. Ratio of model/obs of the daily mean NH$_3$, NH$_4^+$ and total NH$_x$ concentration**
894
895   **Figure 3. Share of major components of gases and particulate matter (PM$_{2.5}$) based on the mean**
896   **concentrations during WiFEX (share according to μeq m^{-3}).**
897
898   **Figure 4. Fraction of HCl/Cl$^-$ ratio as a function of NH$_4^+$ concentration (μg m^{-3}) and Relative humidity (RH)**
899
900   **Figure 5. Bivariate plots of mean (a) NH$_3$ concentration (b) NH$_4^+$ concentration (c) Cl$^-$ concentration and**
901   **(d) total NH$_x$ concentration in relation to wind speed (m s^{-1}) and direction.**
902
903   **Figure 6. Neutralizing effect between Cl$^-$, NO$_3^-$ and SO$_4^{2-}$ as the anions (μeq m^{-3}) and aerosol neutralization**
904   **ratio (ANR) where, ANR>1 indicates over neutralized (alkaline) and ANR<1 indicates under neutralized**
905   **(acid) (orange bar indicates daily mean standard error).**
906
907   **Figure 7. Box-Whiskers plot for trace gases and secondary inorganic aerosols from the observations**
908   **(MARGA) and simulated in sensitivity test with changes in HCl emissions (No HCl (0 mol km^{-2} h^{-1}), Base**
909   **Case HCl (24.8 mol km^{-2} h^{-1}), and 3×Base HCl (74 mol km^{-2} h^{-1})) at IGIA, Delhi.**
910
911   **Figure 8. (top) Average diurnal cycles of NH$_3$ and NH$_4^+$ concentration (μg m^{-3}) with mole equivalents of Cl$^-$**
912   **, NO$_3^-$, SO$_4^{2-}$, NH$_4^+$, SO$_2$, HCl and HNO$_3$ (μeq m^{-3}) of (a) measured (MARGA) and (b) modeled (3×Base HCl**
913   **run) along with its meteorological parameters (bottom).**
914
915   **Figure 9. Diurnal variation in the mean (a) NH$_3$ concentration (b) NH$_4^+$ concentration and (c) total NH$_x$**
916   **concentration observed (black), simulated in No HCl (red dotted), Base Case HCl (red dash) and 3×Base**
917   **HCl run (red solid).**
918
919   **Figure 10. Comparison of ratio of model/obs in the daily mean (a) NH$_3$ concentration (b) NH$_4^+$**
920   **concentration and (c) total NH$_x$ concentration in 3×Base HCl and -3×NH$_3$_EMI scenario.**
921
922
923
924
925
926
927

928 **TABLES**

929 **Table 1. Performance statistics of correlation coefficient (r) of NH_4^+/NH_x with NH_3 and aerosols (NH_4^+, Cl^-**
930 **, SO_4^{2-}, and NO_3^-)**

931

Gases and Aerosols	MARGA Correlation coefficient (r) with NH_4^+/NH_x ratio	Model Correlation coefficient (r) with NH_4^+/NH_x ratio
Ammonia (NH_3)	-0.57	-0.58
Ammonium (NH_4^+)	0.70	0.67
Chloride (Cl^-)	0.79	-
Sulfate (SO_4^-)	0.09	0.77
Nitrate (NO_3^-)	0.13	0.57

932
933
934
935
936
937
938
939
940
941
942
943
944
945
946
947
948
949
950
951
952
953
954
955
956

Table 2. Daily mean ± 1σ in gases and inorganic aerosol concentration observed (MARGA) and simulated in sensitivity test with changes in total HCl emissions (No HCl (0 mol km^{-2} h^{-1}), Base Case HCl (24.8 mol km^{-2} h^{-1}), and 3×Base HCl (74 mol km^{-2} h^{-1}).

Species concentration (µg m^{-3})	MARGA	No HCl	Base Case HCl	3×Base HCl
NH$_3$	20 ± 8.52	50.2 ± 11.7	48.2 ± 11.31	44.5 ± 10.8
NH$_4^+$	35.9 ± 17.7	13.9 ± 3.04	21.4 ± 6.65	34.5 ± 15.2
NH$_x$	56.6 ± 17.1	64 ± 13.2	69.6 ± 16.6	79.5 ± 23.7
Cl$^-$	50.6 ± 39.4	-	15.1 ± 9.65	40.9 ± 27.2
NO$_3^-$	27.9 ± 8.17	35.9 ± 7.23	35.6 ± 7.05	35.5 ± 7.03
SO$_4^{2-}$	17.1 ± 5.63	9.62 ± 2.78	9.56 ± 2.71	9.56 ± 2.71
HCl	0.86 ± 0.35	-	0.20 ± 0.23	0.22 ± 0.25
HNO$_3$	3.43 ± 1.68	0.18 ± 0.21	0.17 ± 0.22	0.18 ± 0.23
SO$_2$	30.6 ± 18.4	46.6 ± 12.4	46.7 ± 12.4	46.7 ± 12.4

979 **Table 3. Model performance statistics for NH_3, NH_4^+ and total NH_x concentration at IGIA, Delhi from three**
980 **sensitivity experiments (No HCl (0 mol km^{-2} h^{-1}), Base Case HCl (24.8 mol km^{-2} h^{-1}), and 3×Base HCl (74**
981 **mol km^{-2} h^{-1})-) and the MARGA**
982

Species	No HCl		Base Case HCl		3×Base HCl	
	Correlation coefficient (*r*)	Normalised Mean Bias (NMB)	Correlation coefficient (*r*)	Normalised Mean Bias (NMB)	Correlation coefficient (*r*)	Normalised Mean Bias (NMB)
NH_3	-0.58	1.38	-0.60	1.29	-0.65	1.13
NH_4^+	0.45	-0.61	0.75	-0.40	0.76	-0.03
NH_x	0.69	0.12	0.70	0.22	0.70	0.39

983
984
985
986
987
988
989
990
991
992
993
994
995

996   **Figure 1**
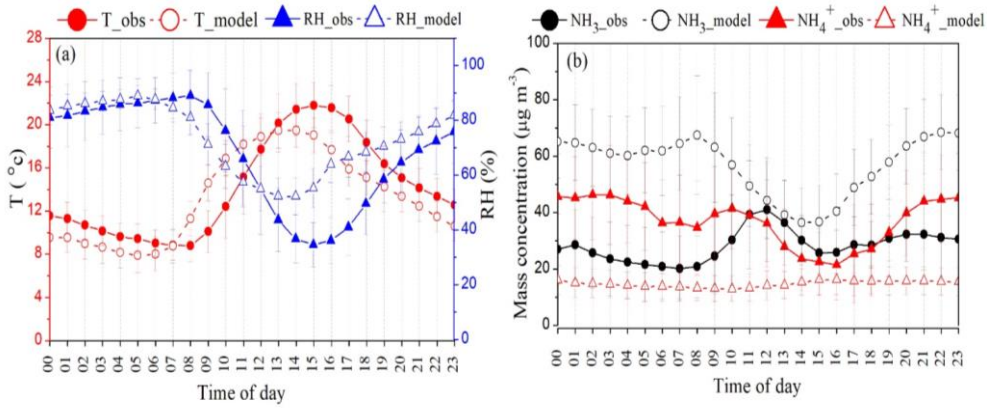
997
998

999   **Figure 2**
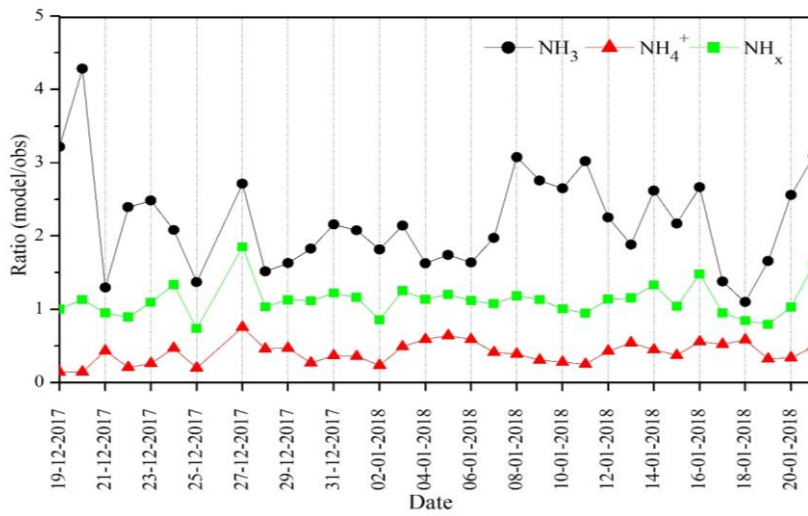
1000
1001
1002
1003

1004   **Figure 3**
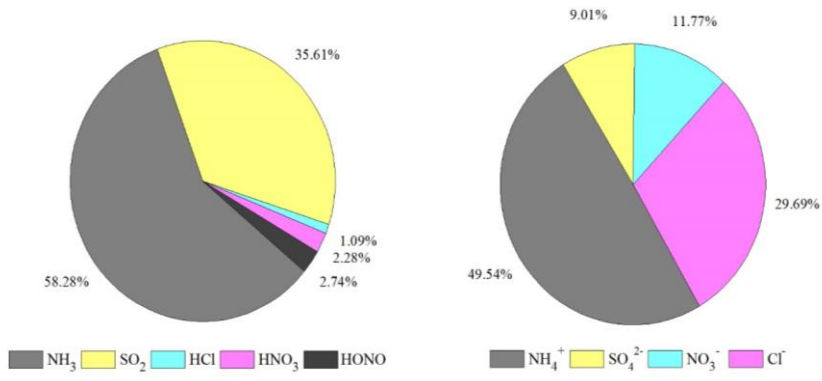
1005
1006
1007

1008   **Figure 4**
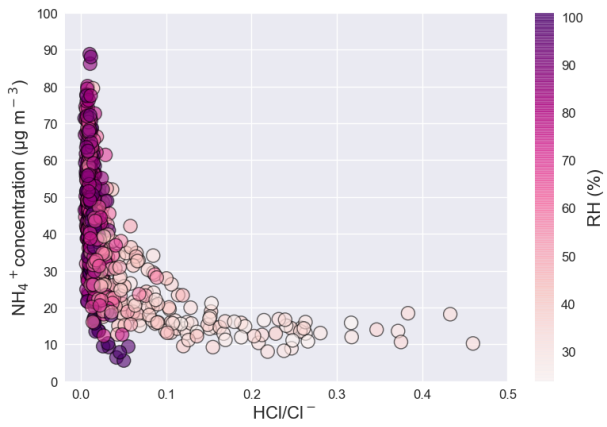
1009
1010

1011

1012

1013   **Figure 5**

Mass concentration ($\mu g\ m^{-3}$)
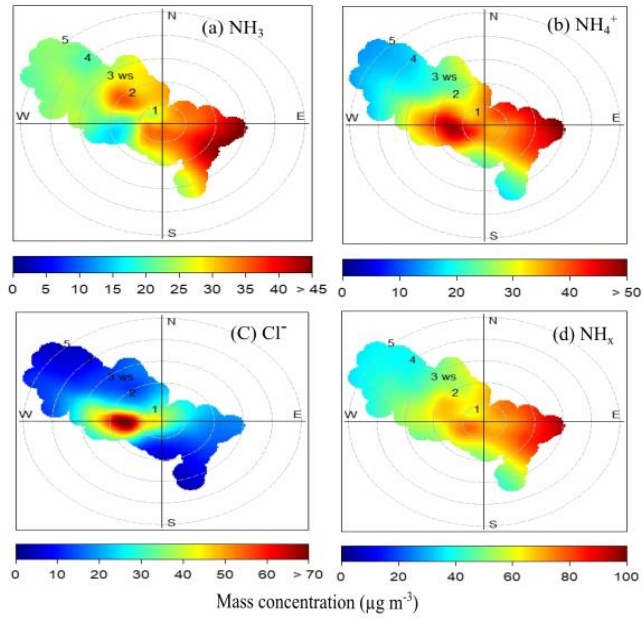
1014

1015   **Figure 6**
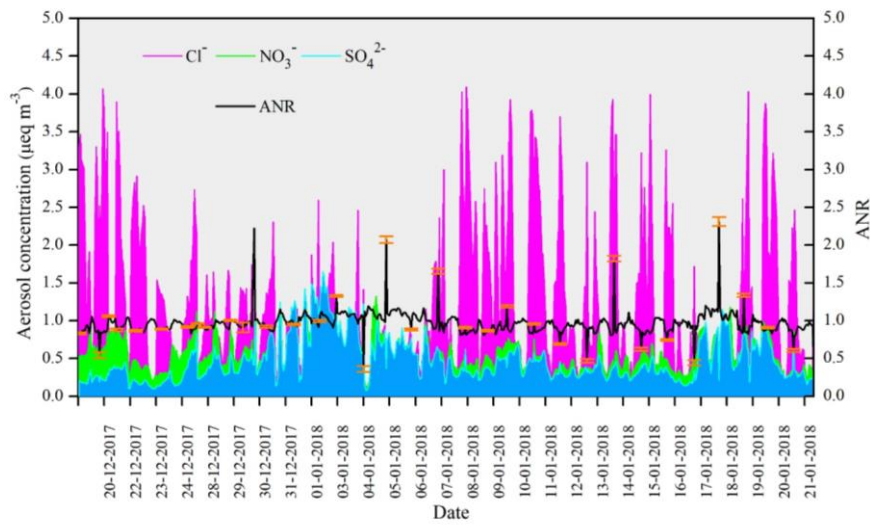
1016

1017   **Figure 7**
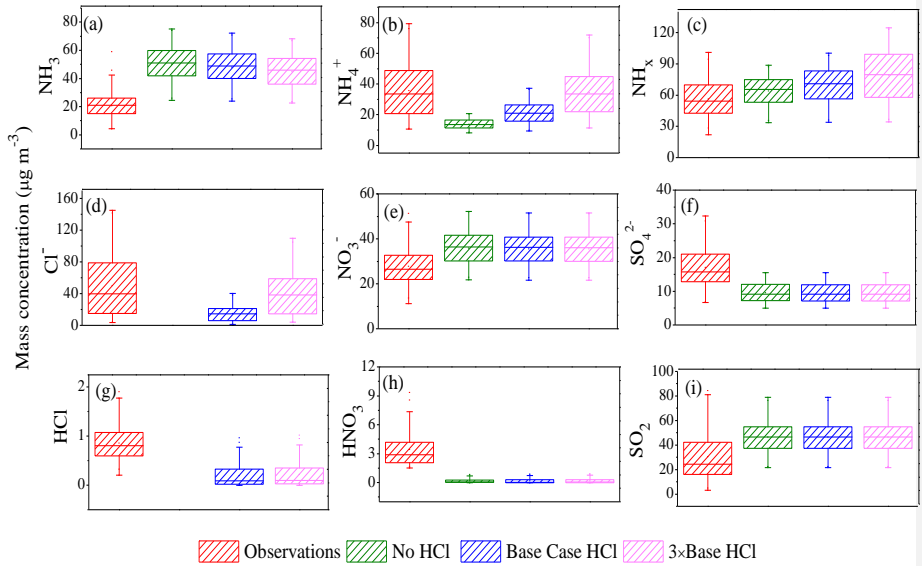
1018
1019   v
1020
1021
1022
1023
1024
1025
1026
1027
1028
1029
1030
1031
1032
1033
1034
1035
1036

1037   **Figure 8**
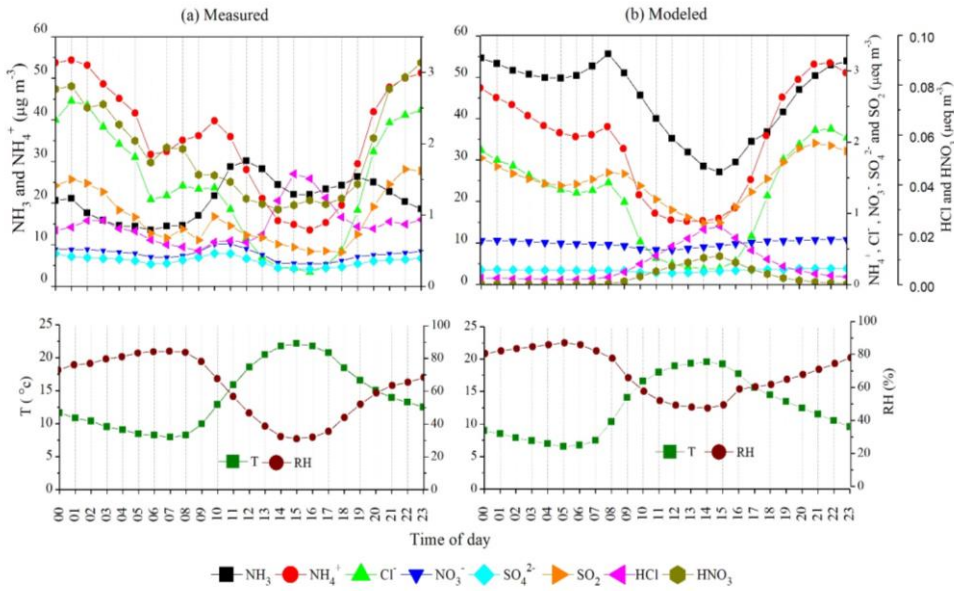
1057 **Figure 9**
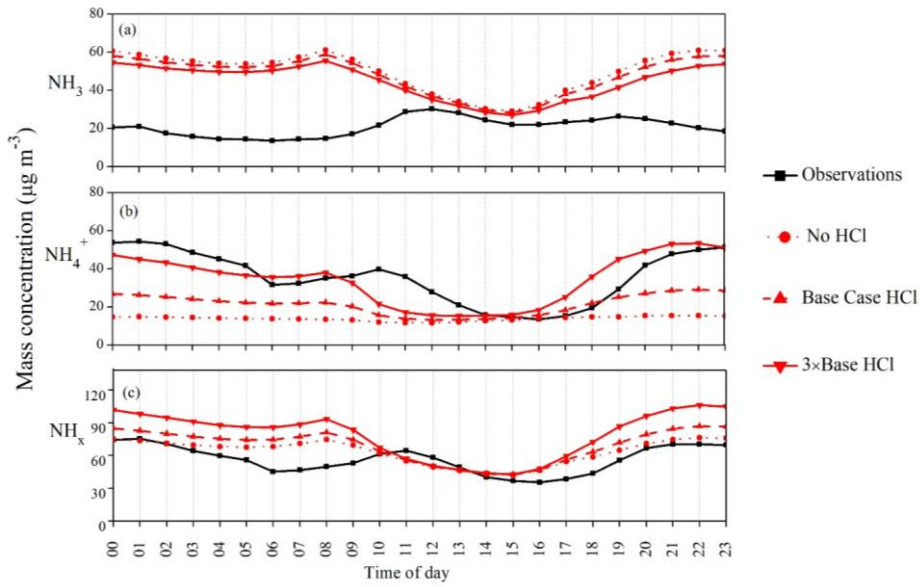
1058

1059

1060

1061

1062

1063

1064

1065

1066

1067

1068

1069

1070

1071

1072

1073

1074   **Figure 10**
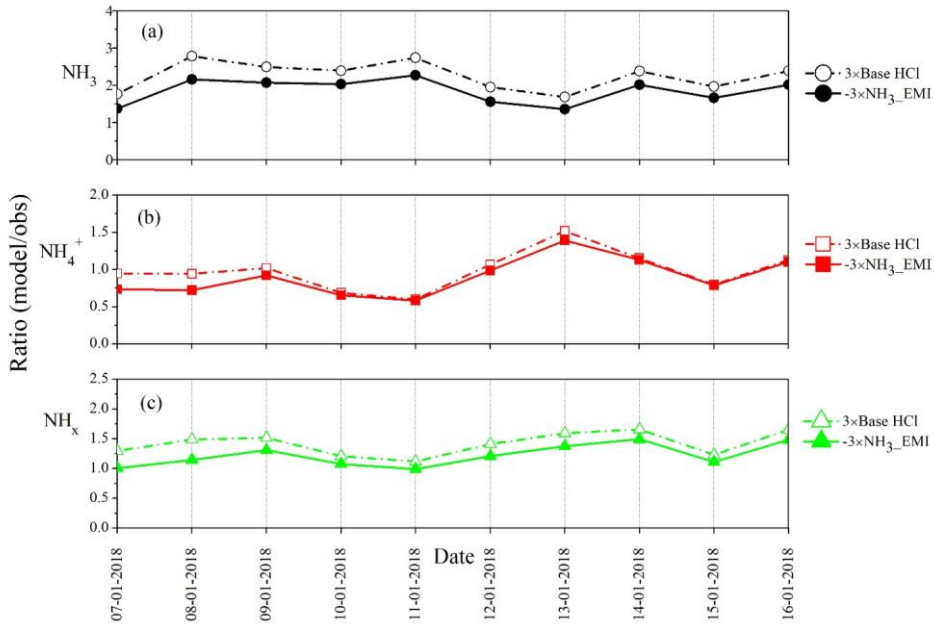
1075
1076
1077
1078
1079
1080
1081
1082
1083